TECHNICAL MEMORANDUM

231

The VIERS 1 scatterometer model

P.A.E.M. Janssen, H. Wallbrink,
C.J. Calkoen, D. van Halsema,
W.A. Oost and P. Snoeij

Research Department

December 1996

European Centre for Medium-Range Weather Forecasts
Europäisches Zentrum für mittelfristige Wettervorhersage
Centre européen pour les prévisions météorologiques à moyen

Abstract

In 1985 a group of four Dutch institutes, combining expertise in radar technology, water waves and meteorology, submitted a proposal to the Netherlands Remote Sensing Board (BCRS) for a systematic study of radar backscatter from the water surface. The study was aimed at the development of a physically based algorithm for the relationship between radar backscatter and the surface wind and would consist of laboratory experiments, experiments at sea from a fixed platform and theoretical studies of the relevant processes. The impetus for the proposal came from the expectation that in a few years time the ERS-1 satellite would be launched with in its AMI package a C-band scaterometer, intended for the measurement of the wind speed and direction at sea from space. The project, which was approved and supported by BCRS, therefore received the name VIERS-1 for Verification and Interpretation ERS-1. It lasted from 1987 until 1994 and has now indeed resulted in the physically based algorithm for which the project was started.

The first experiments in VIERS-1 were done in 1987 in a large wind water flume (length 100 m), where especially the 2D distribution of the small wind waves, which are mainly responsible for radar backscatter, and the radar directional effects of this distribution were studied. An even larger wave tank (length 213 m) was transformed in a wind-wave flume in 1989 to study the effect of long waves on the short ones. In 1990 a final experiment was performed at Meetpost Noordwijk, a research platform 9 km off the Dutch coast, to obtain field data with which to check the model.

The development of that model meanwhile had been started and a computer program was developed, based on state-of-the-art knowledge of radar backscatter, wave modelling and air-sea interaction. Initially a model was made that calculated the radar backscatter under given conditions of wind and sea, later the model was inverted to obtain the wind from the radar backscatter. For operational purposes the model was coupled to the WAM wave model.

The crucial test for VIERS-1 was a comparison of the algorithm with the CMOD4 model, which is mainly based on statistical fitting, using operational data. In this comparison it turned out that the results of VIERS-1 were comparable with those of CMOD4, with VIERS-1 outperforming CMOD4 slightly at both high and low wind speeds, but with CMOD4 providing a somewhat closer fit in backscatter space. This may be interpreted as an appreciable success for VIERS-1: the model is the first of its kind and still has many possibilities for further improvement, whereas CMOD4 is probably the ultimate that can be obtained with a purely statistical approach.

1. INTRODUCTION

Traditionally, the operational retrieval algorithms for the scatterometer which relate the radar backscatter measurements to the surface wind vectors have been empirical. A review of the history of this empirical relationship is given by e.g. *Moore and Fung* (1979), *Jones et al* (1982), *Schroeder et al* (1982) and *Barrick and Swift* (1980). After *Moore and Pierson* (1967) proposed to use a satellite scatterometer's radar echo to determine the wind speed at sea, a variety of early scatterometer models appeared in the 1970's (for example, *Valenzuela et al*, 1971; *Guinard et al*, 1971; *Jones et al*, 1977; *Moore and Fung* 1979 and *Wentz et al*, 1984). The most successful scatterometer model of the early 1980's was the Seasat A Scatterometer System (SASS1) model. The SASS1 model assumed a power law between the radar backscatter σ and wind speed U and was tuned to a subset of the available surface truth wind data from the Joint-Air-Sea Interaction Experiment (JASIN). The wind speed data set was relatively small, 4-16 ms^{-1}. When results of the tuned SASS1 model were compared with the JASIN data not used in the tuning, a favourable agreement was found, giving confidence in the empirical approach. Nevertheless, *Woiceshyn et al* (1986) and *Anderson et al* (1987) pointed out several weak points of the SASS1 algorithm. First of all, low wind speeds were systematically too high while high wind speeds were too low. Secondly, winds obtained from horizontal polarisation were not consistent with vertical polarisation, suggesting that a power law relationship between backscatter and wind is not adequate. Furthermore, it was also felt that other geophysical parameters such as atmospheric stability and water viscosity would have resulted in an improved wind field retrieval, in particular at the lower wind speeds.

Despite the shortcomings, the statistical fitting approach has resulted in a useful algorithm as follows from the work of *Stoffelen and Anderson* (1996), although a somewhat more sophisticated power law relationship needed to be introduced. The resulting backscatter algorithm, called CMOD4, showed a very good fit in backscatter space while, in comparison with ECMWF wind fields, the retrieved wind velocity had a small wind speed error of about 2 m/s and directional error of the order of 20-30 degrees. However, CMOD4 showed for low and high wind speed similar problems as the SASS1 algorithm. When using CMOD4 in ECMWF's analysis system, *Gaffard and Roquet* (1995) found that the underestimation of wind speed in the high wind speed range resulted in less deep lows (by as much as 8 hPa) and, as a consequence, the quality of the atmospheric forecast suffered. By applying a wind speed dependent bias correction to CMOD4 (which was obtained by a comparison with buoy wind speed data) the scatterometer winds were found to have a favourable impact on atmospheric analysis and forecast and even on the ocean wave analysis and forecast (*Andersson et al*, 1996).

Retrieved wind vectors by means of the VIERS scatterometer algorithm are compared in Section 4 with the ECMWF analysed wind fields and it is found that VIERS and ECMWF winds are compatible in a statistical sense. As a reference we use results from CMOD4. A direct comparison between VIERS and CMOD4 winds reveals a good agreement between the two products except that in the high wind speed range VIERS has higher winds than CMOD4 while at low winds VIERS has lower winds. In view of the problems CMOD4 has at the extreme wind speed ranges, it is concluded that the VIERS model is performing better. Nevertheless, it should be emphasized that the misfit in σ_0 space between modelled and observed backscatter is generally larger for VIERS than for CMOD4. This is probably caused by a too simple directional distribution of wind waves in VIERS. After the statistical comparison we proceed with a synoptic discussion of the differences between retrieved and analysed wind concentrating on a frontal system that occurred in the Norwegian Sea on 6 November 1991.

A summary of conclusions is presented in Section 5 and suggestions for improvements are given as well.

2. THE VIERS MODEL

To our knowledge to date, the most successful modelling attempt of the scattering of the radar signal at the sea surface is due to *Donelan and Pierson* (1987). These authors obtained the spectrum of gravity capillary waves from a simplified energy balance, consisting of wind input and dissipation through viscosity and wave breaking. Combining this short wave number with the observed directional spectra of *Donelan et al* (1985) the complete surface wave spectrum is then known.

Scattering off a surface with a broad spectrum of waves is reasonably well modelled by means of a so-called two scale approach (*Valenzuela*, 1978; *Plant*, 1990). Thus, the normalised radar backscatter can be found by integrating the scatter from the individual facets (which are tilted by the longer gravity waves) weighted with the probability that the water surface is tilted by a certain angle. Introducing a separation scale wave number k_c, for high wave numbers ($k>k_c$) the main scattering mechanism is assumed to be Bragg scattering while for $k<k_c$ specular reflection is taken. Results are supposed to be weakly dependent on the choice of k_c; *Donelan and Pierson* (1987) selected $k_c=k_b/40$, where k_b is the Bragg wave number

$$k_b = 2\, k_R \sin\theta_l \qquad (1)$$

with θ_l the local incidence angle which depends on the tilt of the water surface by the long waves and k_R is the radar wave number.

Application of the Donelan and Pierson scatterometer algorithm to the VIERS wave tank data set revealed a number of shortcomings in the model (*Calkoen et al*, 1990). First of all, considerable discrepancies between modelled and observed short wave spectral shape were found; for large winds the modelled spectrum drops off too rapidly while at low wind speed considerable amounts of wave energy were observed beyond the viscous cutoff wave length of Donelan and Pierson. In other words, the modelled Donelan and Pierson short wave spectrum was found to be too sensitive to the effects of water viscosity. Clear experimental evidence of this was also given by *Jähne and Riemer* (1990) who in the framework of the VIERS project measured the slope spectrum by means of optical techniques. Even for low wind speed considerable contributions to the slope spectrum were found at wave number k=800 rad/m which is well-beyond the viscous cut off of Donelan and Pierson. *Apel* (1994) has summarised the findings of *Jähne and Riemer* (1990) and *Klinke and Jähne* (1992) in terms of a semi-empirical model for the short wave spectrum.

Also, shortcomings in the electromagnetics part of the Donelan and Pierson scat algorithm were found. In order to shield off a singularity in the Bragg scattering near nadir, a cutoff condition was applied when the local incidence angle was less than 18°. Nevertheless, for small incidence angle the contribution of Bragg scattering dominates the one of specular reflection, which is unexpected. Furthermore, the choice of the cutoff wave number is not always adequate. For example, for the wave tank data the dominant wave has a much larger wave number than at sea, sometimes even beyond k_c.

In order to alleviate the above-mentioned problems, it was decided to develop a new scatterometer algorithm. In particular, regarding the electromagnetic part, the introduction of a cutoff wave number on a more or less physical basis was considered. Furthermore, it was decided to remove the cutoff condition near nadir and to add the specular reflection. Finally, it was thought to include more physics in the energy balance equation, because nonlinear wave-wave interactions and effects of slicks may be relevant processes as well in determining the short wave spectrum.

Before our attempt to improve on the Donelan and Pierson scatterometer model is described, it is emphasised that a basic assumption of the VIERS scatterometer model is that wind wave generation is determined by the surface stress. At the air sea interface, the stress field is determined by the wind speed, the stability of the air column and the sea state, which we characterise by the wave age of the wind sea. In order to obtain the stress τ or the friction velocity u_*, the wind profile $U(z)$ is assumed to have the form

$$U(z) = \frac{u_*}{k}\,(\log(z/z_o) - \psi(z/L)) \tag{2}$$

Here, the roughness length includes the effects of the sea state and is parametrized according to *Smith et al* (1992)

$$z_o = \alpha\frac{u_*^2}{g},\ \alpha = 0.48(c_p/u_*)^{-1} \tag{3}$$

where c_p/u_* is the age of the wind sea and c_p is the phase speed of the peak of the wind sea spectrum.

For the stability function ψ we adopt the Businger-Dyer expression (*Businger et al*, 1971; *Dyer et al*, 1970):

$$\psi = \begin{cases} -z/L & (\textit{stable};\ L>0) \\ \frac{\pi}{2} + 2\log((1+\Phi)/2) + \log((1+\Phi^2)/2) - 2\tan\phi & (\textit{unstable};\ L<0) \end{cases} \tag{4}$$

where

$$\Phi = (1-16z/L)^{0.25} \tag{5}$$

and the Monin-Obukov length is computed according to *Stewart* (1985),

$$L = \frac{-u_* U(z)}{g\kappa}\,\frac{T_{air}}{T_{sea} - T_{air}} \tag{6}$$

with g the acceleration of gravity, κ the von karman constant, T_{air} the air temperature and T_{sea} the water temperature.

For given wind speed, phase speed of the waves, air and sea temperature the friction velocity u_* is solved from Eq (2) in an iterative manner.

2.1 The short wave model

The model for the short wave spectrum is based on the energy balance equation, which is solved under steady state circumstances because the short waves have a very short response time scale. Also, advection of short wave energy is disregarded and the energy balance equation therefore reads

$$S_{in} + S_{nonl} + S_{visc} + S_{br} + S_{slicks} = 0 \tag{7}$$

where S_{in} represents the effects of wind stress, S_{nonl} describes 3 and 4 wave interactions, S_{visc} describes viscous dissipation, S_{br} describes dissipation due to white capping and S_{slicks} describes the resonant energy transfer between surface waves and slicks (Marengoni effect). The energy balance equation (7) is solved as a boundary value problem in wave number space by providing the energy flux from the long to the short waves at a boundary $k = k_{join} \simeq g/u_*^2$ which corresponds to $c/u_* \simeq 1$ with c the phase speed of gravity waves.

In order to determine the energy flux at the boundary $k=k_{join}$, knowledge of the gravity part of the wave spectrum is required. In general, the long wave spectrum consists of wind sea and swell and the simplifying assumption is made that the energy flux at k_{join} is mainly determined by the wind sea part of the spectrum since swell usually has a small steepness. The one-dimensional wind sea wave number spectrum is assumed to be given by the JONSWAP shape (*Hasselmann et al*, 1973), which is obtained from the frequency spectrum by using the linear dispersion relation for gravity waves. Hence,

$$F(k) = \tfrac{1}{2}\, \alpha_p\, k^{-4} \exp\left[-\frac{5}{4}\left(\frac{k_p}{k}\right)^2\right]\gamma^r \tag{8}$$

where

$$r = \exp\left[\frac{-(k^{1/2}-k_p^{1/2})^2}{2\sigma^2 k_p}\right]$$

In JONSWAP steady state conditions were considered and therefore the spectral parameters k_p, α_p, γ and σ were only determined as a function of dimensionless fetch. The sea state will depend on both duration and fetch, however. In order to accommodate both circumstances, the spectral shape parameters are assumed to depend on the wave age

$$\chi = c_p/u_* \tag{9}$$

where u_* is the friction velocity and c_p is the phase speed of the peak of the wind sea spectrum which in principle may be obtained from an ocean wave prediction model (e.g. the WAM model, cf *Komen et al*, 1994). Thus,

$$\begin{aligned} k_p &= g/c_p^2 \\ \alpha_p &= A\chi^{-B} \\ \gamma &= \max\left[1,\ 1+3\left(1-\left(\frac{0.038}{\chi}\right)^2\right)\right] \\ \sigma &= 0.08 \end{aligned} \tag{10}$$

The parametrization of the Phillips parameter α_p was not obtained from JONSWAP, because in the JONSWAP fit for α_p also laboratory data were used which, as is known from *Donelan et al* (1985), belong to a different family. In a tuning exercise with the full VIERS model it was found that

$$A = 0.24,\ B = 1$$

gave satisfactory results. This choice of parameters for the Phillips parameter is in fair agreement with the reanalysis of JONSWAP data performed by *Günther* (1981). Furthermore, JONSWAP only considered young wind sea cases with a peak enhancement factor γ which was on average 3.3. In order to assure that for old wind sea the JONSWAP spectrum asymptotes to the Pierson Moskowitz spectrum (hence $\gamma \to 1$), we have added the χ^{-2} factor in the expression for γ.

The JONSWAP spectrum is strictly speaking only valid for wave numbers up to 9 times the peak wave number. Recent observations of *Banner* (1989) confirm that up to a wave number of 30 rad/m the wave spectrum indeed follows a k^{-4} law, thus the region of validity of the JONSWAP spectrum may be extended to these high wave numbers. However, the present parametrization of the high wave number tail of the gravity wave spectrum differs in one important aspect from Banner's observations, namely the Phillips parameter shows in the present case a more sensitive dependence on wave age and friction velocity. On the other hand, our parametrization is not in conflict with the data of *Jähne and Riemer* (1990) who found in the Delft wave tank a linear dependence of the gravity wave part of the spectrum on friction velocity which agrees with Eq (10) with $B=1$.

For wave numbers higher than k_{join} a new regime is entered because 3 wave interactions start to play a role in the steady state energy balance of the short waves (Eq (7)). In the following we shall only develop a theory for the one-dimensional wave number spectrum, while the angular distribution of the short waves

is modelled in a fairly simple fashion. The main reason for this is that we were unable to derive a reasonable parametrization of the angular dependence of the nonlinear interactions.

The one-dimensional wave number spectrum $F(k)$, which is related to the Fourier transform of the autocorrelation of the surface elevation, is normalised in such a way that $\int_0^\infty F(k)kdk = E$ where E is the wave variance. The wave energy density $\mathcal{E}$ follows then from

$$\mathcal{E}(k) = \frac{\omega^2}{k} F(k) \tag{11}$$

where we shall only consider pure gravity capillary waves with dispersion relation

$$\omega(k) = \sqrt{gk+Tk^3} \tag{12}$$

with g acceleration of gravity and T surface tension. Hence, effects of current and shear in the current will be neglected.

Let us now describe some of the details of the source terms in the energy balance (7). For the input source term we adopt Plant's expression (*Plant*, 1980),

$$S_{in} = \beta F,\ \beta = \delta\omega\left(\frac{u_*}{c}\right)^2 \tag{13}$$

where the dimensionless constant δ is given the value 0.03. The slowing down of wind by the short waves (the so-called quasi-linear effect) can be incorporated by renormalising δ (cf *Janssen et al*, 1989; *Snoeij et al*, 1993) and it has in practice a considerable effect on the energy balance.

Although Donelan and Pierson did not take effects of nonlinear 3 and 4 wave interactions into account, the work of *Valenzuela* (1978), *van Gastel* (1987) and *Janssen* (1987) suggests that 3 wave interactions play an important role in the dynamical evolution of gravity-capillary waves, while *Kitaigorodskii* (1983) and *Phillips* (1985) stress the importance of 4 wave interactions for short gravity waves. The exact expressions for three and four wave interactions obtained by *Davidson* (1972), *Valenzuela* (1978) and *Hasselmann* (1962) will be used as a guideline to obtain an efficient parametrization of the nonlinear transfer.

Following *Kitaigorodskii* (1983) we assume that the nonlinear transfer is a local process in wave number space and, introducing the energy flux $\varepsilon(k)$ one thus has

$$S_{nl} = -\frac{1}{k}\frac{\partial}{\partial k}\varepsilon(k) \tag{14}$$

and on dimensional grounds the expression for ε reads

$$\varepsilon(k) = \frac{c^4}{v_g}[\alpha_3 B^2 + \alpha_4 B^3] \tag{15}$$

where v_g is the group velocity $\partial\omega/\partial k$, B is the angular average of the degree of saturation (*Phillips*, 1985),

$$B = k^4 F(k) \tag{16}$$

while α_3 and α_4 give the strength of the three and four wave interactions respectively. The coefficients α_3 and α_4 may still depend on the ratio c/v_g. In particular, α_3 should vanish in the gravity wave regime because 3 wave interactions are not possible there.

Three dissipative processes are assumed to play a role in the gravity-capillary regime, namely, viscous dissipation, wave breaking and damping due to slicks. For viscous damping we use the exact expression (*Lamb*, 1934),

$$S_{visc} = -4\nu k^2 F \tag{17}$$

where ν is the kinematic viscosity of water.

Damping by slicks is caused by the Marangoni effect (*Alpers and Hühnerfuss*, 1989) which is the result of a resonant interaction between a sound wave in the surface film and short gravity waves. The Marangoni effect gives rise to an enhanced viscous damping,

$$S_{slicks} + S_{visc} = -4\nu_{eff} k^2 F \tag{18}$$

where

$$\nu_{eff} = \nu M(k, \nu, \delta, E_s) \tag{19}$$

with M a relative damping ratio given by

$$M = \frac{1 + X(\cos\delta - \sin\delta) + XY + Y\sin\delta}{1 + 2X(\cos\delta - \sin\delta) + 2X^2} \tag{20}$$

δ is a phase angle and,

$$X = \left|\frac{E_s}{\rho_w}\right| \frac{k^2}{\sqrt{2\nu\omega^3}}, \quad Y = \left|\frac{E_s}{\rho_w}\right| \frac{k}{4\omega\nu} \tag{21}$$

Furthermore, E_s is the dilational modules of the surface film and ρ_w is the density of water. The surface film is determined by the two parameters δ and E_s. The phase angle δ is approximately 180° whereas E_s depends strongly on the type of slick. For a natural slick, mostly of biological origin, E_s may have the value of 0.01 N/m, whereas for chemical slicks its value may vary between 0.01 and 0.05 N/m.

Slicks may be destroyed, however, by the action of wind. We have modelled this by letting the dilational modules vanish for strong enough winds: $E_s = 0.005(1 - \tanh(10u_* - 4.33))$. In addition, since it is unrealistic that the ocean is covered by a single large slick, a second modification was implemented. Since slicks come in patches, there is need for a fractional filling factor F (*Lombardini*, 1986). With $F \leq 1$ the damping is modified according to $M_F = M/(M+F(1-M))$, where M is the damping when the coverage is complete. Typical F-values are in the range 0.88-0.99.

Individual breaking events are difficult to model because of strong nonlinearity. In a statistical description of wave evolution, the white caps cover only a relatively small fraction and white capping may therefore be regarded as a process which is weak in the mean. In *Komen et al* (1994) it is then shown that the corresponding source term is quasilinear: it consists of the spectrum at the wave number considered multiplied by a factor which is a functional of the entire spectrum. Extending the *Komen et al* (1984) expression for gravity wave dissipation into the gravity-capillary regime we take

$$S_{br} = -\beta_d \, \bar{\omega}(\bar{k}^2 E)^2 (k/\bar{k}) F(k) \tag{22}$$

where β_d is a constant of the order 2, and $\bar{\omega}$ and $\bar{k}$ are mean angular frequency and wave number, while E is the wave variance.

Combining now the explicit expressions for the source terms, the energy balance equation (7) becomes

$$\frac{\partial}{\partial k}\,\varepsilon(k) \;=\; \gamma\,\frac{\omega^2}{k^4}\,B \tag{23}$$

where the parameter γ is defined as

$$\gamma \;=\; \delta\omega\left(\frac{u_*}{c}\right)^2 \;-\; 4\nu M\,k^2 \;-\; \beta_d\,\overline{\omega}(\overline{k}^2E)^2(k/\overline{k}) \tag{24}$$

and hence gives the net effect of wind input and dissipation. The energy flux $\varepsilon(k)$ is given by

$$\varepsilon(k) \;=\; \frac{c^4}{v_g}(\alpha_3\,B^2+\alpha_4\,B^3) \tag{25}$$

and we have eliminated the wave number spectrum F in favour of the degree of saturation $B = k^4F$.

The interaction coefficient α_4 for 4 wave interactions is taken as a constant, $\alpha_4 \approx 0.25$ while α_3 is allowed to depend on wave number because it is assumed that for gravity waves three wave interactions are not important. We take

$$\alpha_3 \;=\; \frac{3\pi}{16}[\tanh\{\sigma_3(x-1)\}+1]$$

where $x = \sqrt{k/k_{join}}$ and $\sigma_3 = 2$. We remark that this choice of α_3 is, to a certain extent, arbitrary; however, a continuous transition from vanishing α_3 in the gravity range to a constant value in the gravity-capillary range is needed to avoid jumps in the spectrum.

By supplying the boundary condition at $k=k_{join}$ of continuity of flux (or spectrum) the differential equation (23) may be solved for the degree of saturation B and the wave number spectrum $F(k)$ follows. In combination with the JONSWAP spectrum for $k<k_{join}$ the full one-dimensional wave number spectrum is obtained. Examples of the one-dimensional wave number spectrum according to the VIERS model equation (23) are shown in Fig 2 for four different friction velocities and old wind sea (wave age $\chi \approx 25$). The sensitive dependence of the high-wave number part of the spectrum on friction velocity should be emphasized; this is of course the main reason why a scatterometer, which 'observes' waves with

wave numbers larger than 100 may be used as an instrument for measuring the wind field above the oceans.

In order to perform a successful wind retrieval, the two-dimensional wave number spectrum is required. To that end, we have taken a simple directional distribution $D(\phi)$,

$$D(\phi) = \frac{1}{2\pi}(1+2a_2\cos 2(\phi-\phi_w)) \tag{26}$$

where ϕ is the wave direction, ϕ_w the wind direction and a_2 a parameter which measures the width of the directional distribution; a_2 is assumed to depend on friction velocity only, and not on wave number. The two-dimensional wave number spectrum is then given by

$$W(k,\phi) = F(k)D(\phi) \tag{27}$$

and it will be used in a two scale model to obtain the normalised backscatter.

2.1.1 *Results of the short wave model*

We would like to discuss briefly some of the properties of the energy balance equation (23). In addition, modelled spectra are compared with observed spectra obtained in the Delft wave tank.

Since in practice the degree of saturation B is of the order 0.1 or less, it is a fair approximation to disregard four wave interactions in the expression for the energy flux, Eq (25). Retaining therefore only three wave interactions, the energy balance equation (23) may be solved and the result for the degree of saturation becomes

$$B = \left(\frac{v_g}{\alpha_3}\right)^{\frac{1}{2}} c^{-2}\left\{\varepsilon_o^{\frac{1}{2}} + \frac{1}{2\alpha_3^{\frac{1}{2}}}\int_{k_{join}}^{k} dk\,\frac{\gamma}{k^2}\sqrt{v_g}\right\} \tag{28}$$

where ε_o is the value of the energy flux at $k = k_{join}$. It is of interest to discuss the respective terms in Eq (28) separately. The first term is related to the effect of three wave interactions. In the absence of wind input and dissipation it follows from the condition of a constant energy flux in wave number space. Using the dispersion relation for pure gravity-capillary waves (Eq (12)) the degree of saturation according to the constant energy flux condition becomes

$$B_{3w} = \left(\frac{\varepsilon_o}{2\alpha_3} \right)^{1/2} c_o^{-3/2} \frac{y(1+3y^2)^{1/2}}{(1+y^2)(y+y^3)^{1/4}} \tag{29}$$

where $y = k/k_o$, $k_o = (g/T)^{1/2}$ is the wave number that separates gravity waves and capillary waves and $c_o = (gT)^{1/4}$. Therefore, in the gravity wave range ($k<k_o$) the degree of saturation increases with wave number like $k^{3/4}$ while, in the capillary wave range, B_{3w} decreases with wave number like $k^{-3/4}$ and B_{3w} attains its maximum value around $k = k_o$.

Effects of wind input and dissipation (γ) are represented by the second term in Eq (28), and result in a modification of the 'inertial' subrange spectrum given in Eq (29). The degree of saturation now becomes a sensitive function of the friction velocity while, for large wave numbers, dissipation becomes important. For a large enough wave number the degree of saturation B will vanish. Let us call this particular wave number the cut-off wave number. In order to be able to compare with results from the Donelan and Pierson model, we shall retain, in γ of Eq (24), only the effects of wind input and viscous dissipation. Hence, the cut-off wave number is determined by viscosity, and the viscous cut-off wave number in the Donelan and Pierson model follows from the condition $\gamma = 0$, or

$$\omega = \frac{1}{4} \frac{\delta u_*^2}{\nu} \tag{30}$$

In the present model, B does not depend on the local value of γ, but on an integral in wave number space involving γ. As a consequence the viscous cut-off wave number shifts to much larger values than given by Eq (30). This shift in cut-off wave number is caused by the nonlinear energy transfer which tries to maintain an inertial subrange spectrum. As a result the present model therefore has a reduced sensitivity to changes in the water viscosity, at least in the wave number range that is relevant for scatterometry.

Furthermore, it is noted that ε_o, which is determined by the JONSWAP spectrum (8), contains all the effects of sea state (i.e. wave age of long waves) on the short wave spectrum. As an illustration, we have compared in Fig 3 the degree of saturation B for young wind sea ($\chi \simeq 7$) with old wind sea ($\chi \simeq 25$), and the sea state dependence may be quite considerable, in particular in the low wave number range. From Fig 3 it is also noted that for young wind sea the increase of B in the high wave number range is less pronounced than in the case of old wind sea, which suggests that for young wind sea the short wave spectrum is controlled by nonlinear transfer because the short gravity waves are steeper.

We conclude this sub-section by comparing results of the present short wave model with observed frequency spectra in the Delft wave tank. Frequency spectra were measured by means of a Lobemeier wire and a laser slope gauge (LSG) of Jähne for different friction velocities and fetches. Lobemeier spectra are thought to be reliable up to a frequency of 10 Hz while LSG spectra are supposed to be valid to at least 100 Hz. If the Doppler shift due to the orbital motion of the long waves is ignored (this is a reasonable assumption in a wave tank), the modelled frequency spectrum $E(f)$ may be obtained from the wave number spectrum $F(k)$ according to

$$E(f) = \frac{2\pi k}{v_g} F(k)$$

where the group velocity v_g is obtained for the dispersion relation of pure gravity-capillary waves (Eq (12)). Examples of the comparison between observed and modelled frequency spectra are shown in Fig 4 for two different friction velocities and a fetch of 90 m. In view of the differences that do exist between the two types of observed spectra, it may be concluded that the present short wave model shows a fair agreement with the observations. Finally, it is remarked that the water surface in the wave tank was clean, hence effects of slicks were disregarded. For low wind speed, slicks may have a dramatic impact on the spectral shape as is illustrated in the low wind speed case of Fig 4.

2.2 The radar backscatter model

Once the 2D wave spectrum is known, the normalised backscatter may be obtained by means of a two-scale model. According to the wave-facet model (*Plant*, 1990), the normalised cross section is given by

$$\sigma_o = \sigma_o^{sp} + \int_{-\infty}^{\infty} d(\tan\psi) \int_{-\infty}^{\infty} d(\tan\delta)\ P_B(\tan\psi,\ \tan\delta)\sigma_o^{Br}(\theta_l) \qquad (31)$$

where P_B is the probability that a (Bragg-) facet is oriented with tilts $\tan\psi$ and $\tan\delta$ along wind and cross wind respectively, while θ_l is the local incidence angle. For an anisotropic Gaussian surface one has

$$P_B = \frac{1}{2\pi s_{u,b} s_{c,b}} \exp\left(-\frac{\tan^2\psi}{2s_{u,b}^2} - \frac{\tan^2\delta}{2s_{c,b}^2} \right) \qquad (32)$$

with $s_{u,b}^2$ and $s_{c,b}^2$ the slope variances in up wind and cross wind. The Bragg contribution of a facet is

proportional to the two-dimensional wave number spectrum at the Bragg wave number k_b (cf Eq (1)). In fact,

$$\sigma_o^{Br} = 8\pi k_R^4 \cos^4\theta_l |g_{pol}|^2 [W(\vec{k}_b)+W(-\vec{k}_b)] \tag{33}$$

with k_R the radar wave number and g a factor which depends on the polarisation. The contribution due to specular reflection is given by

$$\sigma_o^{sp} = \pi |R(o)|^2 \sec^4\theta P(\zeta_x, \zeta_y) \tag{34}$$

where P is the probability that a specular facet is oriented with tilts ζ_x and ζ_y parallel and at right angles to the radar look direction respectively. For an anisotropic Gaussian surface one has

$$P = P(\zeta_x=\tan\theta, \zeta_y=0) = \frac{1}{2\pi s_{u,s} s_{c,s}} \exp\left(-\frac{\tan^2\theta}{2s_{L,s}^2}\right) \tag{35}$$

with $s_{u,s}^2$ and $s_{c,s}^2$ the slope variances in the upwind and crosswind direction, whereas $s_{L,s}^2$ is the variance in the radar look direction. Only those waves that have a wavelength longer than the radar wavelength contribute to the slope variances as shorter waves are not seen by the radar (*Stewart*, 1985). Furthermore, $|R(o)|^2$ is the reflection coefficient at normal incidence, which depends on the radar frequency via the relative dielectric constant ε_r,

$$|R(o)| = |0.65(\varepsilon_r-1)/(\sqrt{\varepsilon_r}+1)^2| \ .$$

The factor 0.65 in this last equation is based on a correction of the standard reflection coefficient as specified by *Valenzuela* (1978). The correction factor is needed because the remaining short wave disturbances of the water surface reduce the cross section as given by physical optics.

The above general two scale theory has to be supplemented with a criterion to separate long waves from short ones. The wave number spectrum is separated into a low and high wave number part by means of the separation scale k_c

$$\begin{aligned} W_L(k, \phi) &= \begin{cases} W(k, \phi), & k < k_c \\ 0, & k > k_c \end{cases} \\ W_H(k, \phi) &= \begin{cases} 0, & k < k_c \\ W(k, \phi), & k > k_c \end{cases} \end{aligned} \tag{36}$$

Hence, using the directional distribution (26) the slope variances of the tilting waves are given by

$$s^2_{u,\,b} = \frac{1 + a_2}{2} \int_0^{k_c} k^3 F(k) dk$$
$$s^2_{c,\,b} = \frac{1 - a_2}{2} \int_0^{k_c} k^3 F(k) dk \qquad (37)$$

while the slope variance of the waves that contribute to specular reflection is given by $s^2_{L,\,s} = s^2_{u,\,b} + s^2_{c,\,b}$. Finally, the separation scale k_c is determined by the condition

$$\beta = 4k_R^2\, \sigma^2_H,\ \sigma^2_H = \int_{k_c}^{\infty} F(k) dk \qquad (38)$$

Condition (38) follows from the work of *Bahar, Barrick and Fitzwater* (1983) and *Brown* (1978). An optimal choice for the parameter β is then found to lie in the range 0.1-1. Based on a comparison with the VIERS dataset (*Snoeij et al*, 1993), β=0.13 turns out to give optimal results for the normalised backscatter.

The present version of the two scale model was tested against observed data obtained during the VIERS tank experiment at Delft Hydraulics. Observed wave spectra were used as input to the backscatter algorithm. Fig 5 shows the normalised radar cross-section σ (in dB) as function of incidence angle for vertical and horizontal polarisation. The fetch was 90 m and the friction velocity was u_*=0.367 m/s. From Fig 5 it is concluded that there is a fair agreement between modelled and observed backscatter for vertical polarisation but that the modelled backscatter is too low by as much as 5 dB for horizontal polarisation.

3. THE INVERSE VIERS MODEL

The VIERS model consists of the three principal components discussed in Section 2, namely 1) a module to determine the stress for given wind, air-sea temperature difference and sea state, 2) a module to determine the short wave spectrum for given stress and sea state of the long wind waves and 3) a module to obtain for given 2-dimensional wave spectrum the normalised backscatter. Therefore, the VIERS model relates radar backscatter to wind vector, measurement geometry (e.g. incidence angle), sea state,

air-sea temperature difference and slicks. In the following we disregard effects of atmospheric stability on the stress.

For the practical application of wind retrieval from (ERS-1) scatterometer data, the model has to be inverted, however. In order to achieve this the following simple, straightforward procedure was adopted.

First a table of normalised backscatter σ_0 is produced; the VIERS model is run for different incidence angles, wind vectors and wave periods (or peak phase speeds) and the resulting σ_0's are collected in a table. The wind parameters are wind speed U and the direction ϕ with respect to the look direction of the radar. If one accepts an accuracy of 1 m/s in retrieved wind speed and 15° in the wind direction, the incidence angle may be chosen in the range of 18° until 57° in steps of 1°, U from 1 until 30 m/s in steps of 1 m/s and ϕ from 15°, for instance.

The inversion procedure we adopted is specific for the ERS-1 configuration, where for a certain cell i three measurements of radar backscatter for different look angle and incidence angle were performed. The measured sigma triplet is denoted by $(\sigma_f, \sigma_m, \sigma_a)$ where the subscripts denote fore mid and aft beam, respectively. The wind retrieval procedure is then as follows

1. Determine incidence angles of fore, mid and aft beam: $\theta_f(i), \theta_m(i), \theta_a(i)$.

2. Calculate the corresponding model triplets for all tabulated wind vectors according to

$$\begin{aligned} \sigma_f^{\mathrm{mod}} &= \sigma^{tab}(\theta_f, U, \phi+45, c_p) \\ \sigma_m^{\mathrm{mod}} &= \sigma^{tab}(\theta_m, U, \phi, c_p) \\ \sigma_R^{\mathrm{mod}} &= \sigma^{tab}(\theta_a, U, \phi-45, c_p) \end{aligned} \tag{39}$$

Here, ϕ is the wind direction with respect to the midbeam and c_p is the wind sea phase speed obtained from a wave prediction model (e.g. the WAM model, *Komen et al*, 1994).

3. Determine the normalised quadratic distance between modelled and measured triplets,

$$Q_{ERS\text{-}1} = \sum_{n=1}^{n_b} Q_n \tag{40}$$

where the index n refers to the beam (n_b=3) and

$$Q_n = \left(\frac{\sigma_n - \sigma_n^{\mathrm{mod}}}{k_p \sigma_n} \right)^2 \tag{41}$$

Here, k_p is the relative accuracy of the measurement (of the order of 5%) and $k_p\sigma_n$ is the measurement error in σ.

4. Determine the normalised quadratic distance between retrieved and ECMWF wind (both magnitude and direction),

$$Q_{GEO} = \left(\frac{U - U_{GEO}}{\Delta U_{GEO}} \right)^2 + \left(\frac{\phi + \chi_m - \phi_{GEO}}{\Delta \phi_{GEO}} \right)^2 \tag{42}$$

where χ_m is the look direction of the midbeam with respect to north. The errors in the ECMWF wind fields are estimated to be $\Delta U_{GEO} = 2\ m/s$ and $\Delta \phi_{GEO} = 20^o$.

5. Determine for all 30x24 tabulated wind vectors the cost function D,

$$D = \sqrt{Q_{ERS\text{-}1} + Q_{GEO}} \tag{43}$$

and infer its absolute minimum.

6. The model wind that minimises D is called the retrieved wind. The wind direction with respect to true North, ϕ_w, is given by $\phi_w = \chi_m + \phi_{ret}$, where ϕ_{ret} is the retrieved wind direction with respect to the midbeam.

The fourth step is inserted in order to remove the ambiguity in direction of 180°. This is a well-known problem in scatterometry and is evident from expression (33) of the Bragg contribution to the radar backscatter. Thus, the ambiguity problem is removed by step 4 but one may introduce a spurious interdependence between retrieved and ECMWF winds.

Before we discuss in the next section results for wind retrieval with the VIERS algorithm, it is of importance to briefly comment on the tuning procedure we followed. Several parameters in the short wave model are not fixed a priori, the most important ones being k_{join}, the directional width parameter a_2

and the Phillips parameter α_p. However, it should be emphasized that there are empirical guidelines for the choice of a_2 and α_p. Nevertheless, the model output depends critically on the precise choice of k_{join}, a_2 as a function of u_* and α_p as a function of wave age. These three variables were the basic tuning parameters.

Initially, we tuned the 'forward' VIERS algorithm. Thus, the simulated backscatter, obtained using ECMWF winds and WAM model periods, was compared with the backscatter as observed by ERS-1. After some tuning a reasonable agreement between simulated and observed backscatter was obtained. We typically found a standard deviation of error of about 2 dB in σ_0, which in view of the limited knowledge of the spectrum of short waves and in view of the accuracy of the analysed wind field (which we assume to be 2 m/s) is already quite an achievement. We were therefore quite optimistic that the thus obtained algorithm would be successful in retrieving winds from the observed radar backscatter. Unfortunately, this turned out not to be the case and some additional tuning was required to obtain reliable winds. The main reason for the additional tuning is that we needed an accuracy of the model algorithm of at least 0.5 dB which cannot be achieved using analysed winds with a relatively large error in magnitude (± 2 m/s) and direction (± 15°).

It was therefore decided to use the inverse of the VIERS model to do the tuning. To that end, about 30 000 σ_0 triplets, measured with the ERS-1 scatterometer on 6 November 1991, together with collocated periods from the WAM model, were supplied to the inverted VIERS model. The resulting retrieved winds (magnitude and direction) were plotted against collocated analysed winds obtained from the ECMWF atmospheric model. The tuning parameters k_{join}, a_2 and α_p were chosen in such a way that the average bias and scatter index (between VIERS and ECMWF winds) were as low as possible and the spectra from the short wave model of the best quality. This approach ensures that the VIERS and ECMWF winds are compatible in a statistical sense, while also reasonable choices for the tuning parameters have been obtained. For example, the wave age dependence of the Phillips parameter, as given in Eq (10), is in fair agreement with Günther's reanalysis of the JONSWAP data.

The tuned VIERS algorithm has been used to produce the plots depicted in Figs 6 and 7. In order to visualize the density of points, contour lines of equal density (number of points per square m/s cq°) are drawn. As a reference we have produced the same plots with the CMOD4 model, using the same inversion technique. It can be seen that the VIERS is well-tuned in the sense that it produces winds that are compatible with the analysed ECMWF winds.

4. WIND RETRIEVAL WITH THE VIERS ALGORITHM

In this section we would like to present our results for wind retrieval with the VIERS algorithm. Results are compared in detail with analysed wind fields from ECMWF and with retrieved winds from the CMOD4 algorithm. Two approaches are followed. In section 4.1 we shall use statistical tools to compare results, while in section 4.2 we give a comparison of results with emphasis on synoptic situations. It is felt that these two approaches are to some extent complementary and they will highlight the strong and weak points of the VIERS algorithm.

4.1 **Statistical comparison**

We have applied the wind retrieval algorithms of VIERS and CMOD4 to three cases on 6 and 7 November 1991 and 10 March 1992 all on 12Z. To that end we collocated the σ_0 triplets, as measured by the ERS-1 scatterometer with wave periods of the WAM model and with analysed wind fields from the ECMWF atmospheric model.

As a first result we compare retrieved wind speed and direction from VIERS with the analysed ECMWF winds. The comparison for the three dates is shown in Figs 6-11. As a reference the same plots are produced with CMOD4 using the same inversion technique as VIERS. As already discussed, we have performed fine tuning of the VIERS algorithm on the 6 November case. The results of the two other dates show that the tuning procedure was robust. Although the standard deviation of error on these last two dates has increased somewhat, it should be noted that for CMOD4 a similar remark applies.

Statistical parameters for the three dates are summarised in Table 1. Regarding the wind vector, the statistics of VIERS and CMOD4 are comparable, with VIERS having slightly better directional properties. However, as may be inferred from Figs 6, 8 and 10, CMOD4 does not allow wind speeds below 2 m/s and this may contribute to more favourable statistics. Furthermore, CMOD4 seems to underestimate the wind speed for high winds. In order to see this point more clearly, we have restricted the determination of the statistical parameters to those cases where the analysed ECMWF wind was higher than 15 m/s. Results are given in Table 2.

The statistics in Table 2 show that both retrieval algorithms are biased low, but that CMOD4 clearly underestimates the wind speed. It is emphasized that an underestimation of wind speed at high winds is an undesirable property of a retrieval algorithm. As shown by *Gaffard and Roquet* (1995), when used in an atmospheric data assimilation scheme, the retrieved winds could result in a considerable slowing down of the major storm systems. Of course, our conclusion on the weak performance of CMOD4 at high winds

MODEL	VIERS	CMOD4	VIERS	CMOD4	VIERS	CMOD4
DATE	911106	911106	911107	911107	920310	920310
number	29752	29752	25771	25771	30049	30049
μ_u (m/s)	-0.08	-0.02	+0.02	+0.10	+0.10	+0.07
σ_u (m/s)	2.04	2.04	2.20	2.20	2.35	2.43
μ_ϕ (°)	+1.6	-3.2	-0.5	-4.4	0	-1
σ_ϕ (°)	28	33	29	31	24	26
D_σ	5.2	3.8	5.9	3.9	5.4	3.7
σ_R (m/s)	0.75	0.47	0.80	0.47	0.69	0.49

Table 1: Statistical comparison of VIERS and CMOD4 winds against ECMWF analysed winds. (Here, μ refers to the bias and σ is the standard deviation). Also, the distance between modelled and observed backscatter is given, as well as the anticipated error in wind speed caused by the misfit in σ_0-space.

MODEL	VIERS	CMOD4	VIERS	CMOD4	VIERS	CMOD4
DATE	911106	911106	911107	911107	920310	920310
number	1324	1324	1124	1124	1237	1237
μ_u (m/s)	-0.89	-2.56	-2.18	-3.04	-0.14	-1.26
σ_u (m/s)	2.02	2.02	2.13	2.51	2.55	2.44
μ_ϕ (°)	-3.2	-4.8	-6.2	-6.8	4.9	4.2
σ_ϕ (°)	12.3	11.5	14.8	15.4	15.5	15.0
D_σ	5.1	3.6	4.5	3.0	4.7	3.6
σ_R (m/s)	1.14	0.60	0.84	0.52	0.98	0.71

Table 2: Same as Table 1 but now under the restriction that the ECMWF windspeed is bigger than 15 m/s.

depends on the quality of the analysed ECMWF winds. However, *Gaffard and Roquet* (1995) also compared CMOD4 wind speeds with quality controlled buoy wind measurements over a 2 year period. The data set was provided by Météo-France and consisted of buoy reports received through the GTS which are closer than 100 km in space and 3 hours in time to scatterometer measurements. CMOD4 was found to overestimate wind speeds in the low wind speed range by about 1 m/s while in the high wind speed range CMOD4 underestimated wind speed by as much as 2 m/s or even larger. Based on the comparison between CMOD4 and the buoy observations, *Gaffard and Roquet* (1995) applied a wind speed dependent bias correction to the wind speeds retrieved by CMOD4 and, in comparison with the ECMWF first-guess winds, hardly any bias was found in the wind speed range up to 20 m/s. When the corrected CMOD4

winds were used in ECMWF's analysis system an improved agreement between Radar Altimeter wind speeds and analysed wind speed was found, while also the forecast showed improvements.

It is therefore concluded that for high wind speeds the VIERS algorithm performs better than CMOD4. A similar remark applies to the low wind speed cases. A summary of the difference in wind retrieval of VIERS and CMOD4 is given in Fig 12. The differences at low and high wind speed confirm the picture we have sketched above. Finally, Roquet (private communication, 1995) compared retrieved VIERS winds with the buoy data and found a good agreement, in particular at high wind speeds.

It is emphasized that high wind cases usually correspond to young wind sea because the time scale to reach equilibrium condition is proportional to wind speed. One of the reasons to develop the VIERS algorithm was that it was expected that the radar backscatter depends on the sea state. Young wind waves are usually steeper than old wind waves and therefore for the same wind speed a larger backscatter would result (cf Fig 3). However, if one would not take the sea state dependence of the radar backscatter into account (by taking for example a fixed wave age $c_p/u_* = 35$), then the short waves would be less steep, giving for the same wind a smaller backscatter. As a consequence, with the same observed backscatter one would expect larger winds in a sea-state independent algorithm. This turns out to be the case. We reran the VIERS algorithm in sea-state independent mode by fixing the wave age c_p/u_* to a constant value, $c_p/u_* = 35$. We took the period of 6 November 1991 and we restricted the wind retrieval to those cases where the ECMWF wind speed is larger than 15 m/s. When comparing the thus obtained retrieved winds with analysed winds we found, as expected, a positive bias of 1.64 m/s while the standard deviation of error was 2.74 m/s which is considerably larger than obtained from the sea state dependent version of VIERS (cf Table 2). It is concluded from this comparison that the sea state dependence of radar backscatter has a considerable impact on wind retrieval. It gives rise in a change of bias of 2.5 m/s. Moreover, in view of the smaller standard deviation of error, we conclude that a sea state dependent backscatter algorithm is to be preferred.

In order to finish our discussion on the performance of the VIERS algorithm, we finally concentrate on its properties in the so-called σ-space. The σ-space is the space spanned by the radar backscatter of fore, mid and aft beam. Let us introduce the distance D_σ in σ-space as

$$D_\sigma = \sqrt{Q_{ERS\text{-}1}} \tag{44}$$

where $Q_{ERS\text{-}1}$ is given by (40) then, ideally, a perfect model should have a distance which is as small as possible, i.e. D_σ=0. There are two reasons why in practice D_σ attains a finite value. The first reason is finite measurement errors. Assuming that there is no bias between model and observation, $\langle \sigma_{obs} - \sigma_{mod} \rangle = 0$, and assuming that the backscatter model is perfect one obtains, using (41),

$$\langle Q_n \rangle = 1$$

and therefore the minimal distance in σ-space becomes

$$D_\sigma = \sqrt{3}$$

Assuming, in addition, that the variable $\delta = (\sigma_{obs} - \sigma_{mod})/k_p \sigma_{obs}$ is a Gaussian variable then for a perfect model the distribution of the distance D_σ can be calculated. Thus, the statistics of D_σ are determined by 3 independent Gaussian variables δ_f, δ_m and δ_a with $\langle \delta \rangle = 0$ and $\langle \delta^2 \rangle = 1$. In that event the distribution of D_σ^2 is chi-square with 3 degrees of freedom. This result is valid if the assumption of independent Gaussian variables is justified and if the model at hand is perfect.

In practice, the actual distribution may deviate from the theoretical one, however. The discrepancy is caused by random model errors (assuming that all systematic errors have been eliminated) that broaden the distribution of δ. As a result, in practice the mean distance $\langle D_\sigma \rangle$ may be larger than $\sqrt{3}$ and the distribution of D_σ^2 may be different from the chi-square distribution. In Tables 1 and 2 we show the mean

values of D_σ for VIERS and CMOD4 and evidently CMOD4 fits the observed backscatter more closely. This conclusion is supported by Fig 13 where we have plotted the distribution of D_σ for CMOD4 and the VIERS model. The period was 6 November 1991. The distribution for a perfect model is shown as well. We note from Fig 13 that CMOD4 has a more narrow distribution than VIERS but both model distributions deviate considerably from the one of a perfect model.

Assuming that the model function describes reality in a reasonable manner, it is even possible to infer the rms error of the retrieved wind speed from the misfit in σ-space. Of course, a misfit in σ-space will induce an error in both wind speed and direction. It is known, however, that the mean of the backscatter from fore and aft beam,

$$x = \tfrac{1}{2}(\sigma_a+\sigma_f)$$

is to a good approximation independent of the azimuth angle. This readily follows, assuming Bragg scattering, from the directional wave spectrum, given by Eq (27), which involves a $\cos(2\theta)$ where θ is the difference between azimuth angle and wind angle. Since the azimuth angle for the fore and aft beam is 90° apart, it follows that the sum of fore and aft beam backscatter is independent of azimuth angle. The error in wind speed then immediately follows from

$$\delta x = \frac{\partial x}{\partial U_{10}}\,\delta U_{10}$$

where δx is the difference between modelled and observed mean backscatter and the derivative of x with respect to U_{10} can be obtained at the minimum distance D by finite differencing. By averaging the square of the error δU_{10} over all retrievals the overall rms error in wind speed σ_R may be determined according to

$$\sigma_R = \sqrt{<\delta U_{10}^2>}$$

Results of this calculation are shown in Tables 1 and 2. According to this estimate VIERS has an rms error in wind speed of about 0.75 m/s and CMOD4 has an rms error of 0.5 m/s, while for the high wind speed cases of Table 2 we get 1 m/s and 0.6 m/s respectively.

All in all, it is difficult to decide which algorithm is better. On the one hand, CMOD4 has a smaller rms error in wind speed because the misfit in σ-space is smaller than for VIERS. On the other hand, when compared to buoy observations and ECMWF analyses, CMOD4 underestimates wind speed considerably while VIERS has less problems in that respect. We therefore conclude that the VIERS model is an acceptable model to retrieve the wind vector from radar backscatter measurements.

Although the VIERS model seems to perform in a reasonable manner, it is still of interest to discuss possible reasons for the larger misfit in σ-space. An important factor could be the choice of the directional distribution of waves. In VIERS (cf Eq (26)) we use a rather simple direction spectrum with a friction velocity dependent width. From observations it is known that the width also depends on the ratio of wave number to peak wave number of the spectrum (*Donelan et al*, 1985). In addition, *Jähne and Riemer* (1990) have observational evidence for a bimodal distribution. In order to see to what extent the directional distribution of the waves plays a role in the wind retrieval, it was decided to do a retrieval experiment using only the fore and aft beam, since the mean of fore and aft beam backscatter is approximately independent of the directional distribution. A much better fit of the VIERS model to the observed backscatter was obtained in this manner. The resulting wind speed error obtained from the misfit in σ-space now becomes only 0.5 m/s. After the VIERS project was finished, Wallbrink and Janssen (private communication, 1996) improved the directional distribution and were able to obtain a

values of D_σ for VIERS and CMOD4 and evidently CMOD4 fits the observed backscatter more closely. This conclusion is supported by Fig 13 where we have plotted the distribution of D_σ for CMOD4 and the VIERS model. The period was 6 November 1991. The distribution for a perfect model is shown as well. We note from Fig 13 that CMOD4 has a more narrow distribution than VIERS but both model distributions deviate considerably from the one of a perfect model.

Assuming that the model function describes reality in a reasonable manner, it is even possible to infer the rms error of the retrieved wind speed from the misfit in σ-space. Of course, a misfit in σ-space will induce an error in both wind speed and direction. It is known, however, that the mean of the backscatter from fore and aft beam,

$$x = \tfrac{1}{2}(\sigma_a+\sigma_f)$$

is to a good approximation independent of the azimuth angle. This readily follows, assuming Bragg scattering, from the directional wave spectrum, given by Eq (27), which involves a $\cos(2\theta)$ where θ is the difference between azimuth angle and wind angle. Since the azimuth angle for the fore and aft beam is 90° apart, it follows that the sum of fore and aft beam backscatter is independent of azimuth angle. The error in wind speed then immediately follows from

$$\delta x = \frac{\partial x}{\partial U_{10}}\,\delta U_{10}$$

where δx is the difference between modelled and observed mean backscatter and the derivative of x with respect to U_{10} can be obtained at the minimum distance D by finite differencing. By averaging the square of the error δU_{10} over all retrievals the overall rms error in wind speed σ_R may be determined according to

$$\sigma_R = \sqrt{<\delta U_{10}^2>}$$

Results of this calculation are shown in Tables 1 and 2. According to this estimate VIERS has an rms error in wind speed of about 0.75 m/s and CMOD4 has an rms error of 0.5 m/s, while for the high wind speed cases of Table 2 we get 1 m/s and 0.6 m/s respectively.

All in all, it is difficult to decide which algorithm is better. On the one hand, CMOD4 has a smaller rms error in wind speed because the misfit in σ-space is smaller than for VIERS. On the other hand, when compared to buoy observations and ECMWF analyses, CMOD4 underestimates wind speed considerably while VIERS has less problems in that respect. We therefore conclude that the VIERS model is an acceptable model to retrieve the wind vector from radar backscatter measurements.

Although the VIERS model seems to perform in a reasonable manner, it is still of interest to discuss possible reasons for the larger misfit in σ-space. An important factor could be the choice of the directional distribution of waves. In VIERS (cf Eq (26)) we use a rather simple direction spectrum with a friction velocity dependent width. From observations it is known that the width also depends on the ratio of wave number to peak wave number of the spectrum (*Donelan et al*, 1985). In addition, *Jähne and Riemer* (1990) have observational evidence for a bimodal distribution. In order to see to what extent the directional distribution of the waves plays a role in the wind retrieval, it was decided to do a retrieval experiment using only the fore and aft beam, since the mean of fore and aft beam backscatter is approximately independent of the directional distribution. A much better fit of the VIERS model to the observed backscatter was obtained in this manner. The resulting wind speed error obtained from the misfit in σ-space now becomes only 0.5 m/s. After the VIERS project was finished, Wallbrink and Janssen (private communication, 1996) improved the directional distribution and were able to obtain a

misfit in σ-space that was similar to the one of the CMOD4 algorithm, but the quality of the wind retrieval product remained the same.

4.2 Synoptic validation using CAL/VAL data

In this section we shall discuss in some detail results of another method of validating the retrieved wind fields obtained with the VIERS model, namely we compare windfields from VIERS with those of a meteorological model and CMOD4. Although this synoptic validation is only qualitative, it has a certain number of advantages over a statistical validation:

1. One can easily verify by eye the internal consistency of the wind speed and directions of adjacent scatterometer cells; in addition it is fairly straightforward to identify ambiguity errors and incidence angle dependent problems in the algorithm.
2. One can directly compare the structure of the wind fields of ERS-1 derived wind fields and model derived wind fields.

4.2.1 *The calibration and validation campaign*

When ESA distributed an Announcement of Opportunity for the calibration and validation of the sensors and products of ERS-1, the VIERS group submitted a proposal for the validation of the wind scatterometer product. This proposal was granted by ESA and access was given to the Calibration and Validation data acquired during the CalVal campaign in the Norwegian part of the North Sea and the Atlantic Ocean between 5°W and 10°E and 60° and 70°N in 1991. ESA was the initiator of this large campaign in which information on the ocean and weather conditions was acquired during overpasses of the ERS-1 satellite. At that time the satellite was in a three day repeat period orbit which had a scatterometer cross-over point west of Norway.

The data acquired from the in situ sensors and other sensors were used together with those of the Norwegian meteorological model (called METEO from now on) to provide the best possible estimate of

the wind field over the scatterometer swath during the passage of the satellite. Besides the ERS-1 measured triplets of the radar scattering at the ocean surface, the VIERS model needs to have the peak frequency of the wind sea part of the dominant waves as input. This parameter was obtained from output of the operational WAM model at KNMI, which was kindly provided by J Onvlee.

Retrieved VIERS winds were then generated by running the inverse VIERS model using the collocated Meteo winds as side condition. In a similar fashion CMOD4 retrieved winds were obtained. The resulting winds were imaged on a plane tangential to the earth at 65 degrees north and 5 degrees east. An example is given in Fig 14. Here wind speed is coded by a colour scale, where the scale ranges from 0 to 24 m/s while the arrows in the plot indicate the flow direction.

Table 3 presents an overview of the data used. It lists mean wind speeds, the differences between model and ERS-1 derived winds as well as the differences between VIERS and CMOD4. Assuming neutral conditions, the average difference between VIERS and METEO is 0.8 m/s and between CMOD4 and METEO +0.3 m/s. The standard deviation of the difference between VIERS and METEO is 2.3 m/s and 2.0 m/s for CMOD4 and METEO. If unstable conditions are assumed, which is the usual condition for this part of the ocean in the autumn, then the mean difference between VIERS and METEO reduces to 0.1 m/s. The differences between VIERS and CMOD4 are much smaller than between each of them with the METEO winds.

Date	METEO	VIERS	CMOD4	VIERS-METEO		CMOD4-METEO		VIERS-CMOD4	
		neutral		avg	std	avg	std	avg	std
910919a	11.6	10.1	10.1	-1.5	1.4	-1.4	1.2	-0.1	0.6
910922a	14.1	9.3	8.6	-4.8	2.4	-5.5	2.5	0.8	0.7
910928a	5.9	6.0	6.2	0.1	2.0	0.3	1.9	-0.2	0.6
911007a	10.9	11.1	10.8	0.2	3.3	-0.0	3.1	0.3	0.6
911010a	7.4	7.3	7.5	-0.2	1.6	0.0	1.5	-0.2	0.5
911019a	9.9	13.6	12.9	3.7	1.5	3.1	0.9	0.6	0.8
911022a	9.9	11.5	11.8	1.5	1.6	1.9	1.2	-0.4	0.7
911028a	5.4	4.9	5.0	-0.5	1.4	-0.4	1.2	-0.1	0.5
911103a	6.4	7.8	7.8	1.4	3.0	1.4	2.3	0.0	1.1
911106a	3.1	3.4	4.1	0.3	1.8	0.9	1.7	-0.6	0.7
911112a	6.5	7.8	8.1	1.3	1.9	1.6	1.8	-0.3	0.6
911115a	2.0	4.3	4.7	2.3	2.1	2.7	1.7	-0.4	0.8
911121a	13.2	17.1	15.6	3.8	3.1	2.4	3.0	1.4	1.1
911124a	11.4	14.6	14.1	3.2	4.3	2.7	4.3	0.5	1.0
911130a	14.4	14.4	13.6	0.0	2.8	-0.8	2.2	0.8	0.8
911203a	11.2	13.5	13.2	2.3	1.1	2.0	1.1	0.3	0.6
911209a	8.9	9.9	10.2	1.0	2.4	1.3	2.1	-0.3	0.7
910918b	13.2	10.7	10.0	-2.5	3.5	-3.2	3.4	0.7	1.1
910924b	10.2	10.2	9.1	-0.1	4.0	-1.1	3.8	1.1	1.0
910927b	5.8	5.9	6.1	0.1	2.8	0.3	2.4	-0.2	1.0
911003b	11.6	10.5	9.8	-1.1	2.2	-1.8	2.1	0.7	1.4
911006b	7.7	8.2	7.9	0.5	1.6	0.2	1.1	0.3	1.2
911012b	4.1	5.5	5.5	1.5	3.0	1.4	2.4	0.0	1.2
911015b	2.8	2.8	3.7	0.0	1.7	0.9	1.2	-0.9	1.1
911021b	6.9	9.7	9.5	2.8	1.9	2.6	1.6	0.2	0.9
911024b	7.3	7.2	7.4	-0.0	1.9	0.1	1.6	-0.2	0.9
911030b	12.0	6.7	6.6	-5.3	3.3	-5.4	2.7	0.1	1.1
911102b	8.9	9.1	8.2	0.2	2.0	-0.7	1.5	0.8	1.0
911108b	8.4	9.3	9.4	1.0	2.2	1.0	1.6	-0.0	1.3
911111b	11.2	13.4	12.1	2.2	1.9	0.8	1.6	1.4	1.1
911117b	4.7	7.3	7.1	2.6	2.9	2.5	2.3	0.2	1.2
911126b	12.0	13.9	12.4	1.8	2.5	0.4	2.0	1.5	1.4
911202b	12.3	14.9	13.2	2.6	2.0	0.9	1.6	1.7	1.2
911205b	7.2	7.9	7.9	0.7	1.6	0.7	1.3	0.1	1.0
910919c	12.5	16.5	14.0	4.0	1.1	1.5	1.3	2.5	1.2
910922c	5.2	5.7	6.2	0.5	3.9	1.0	3.5	-0.5	1.2
910928c	5.2	6.1	6.0	0.9	2.2	0.8	1.4	0.1	1.2
911001c	10.9	12.4	11.4	1.5	1.9	0.5	1.6	1.0	1.2
911007c	11.2	11.3	10.1	0.1	2.4	-1.1	1.7	1.1	1.3
911010c	10.1	10.0	9.2	-0.0	1.5	-0.9	1.1	0.9	1.1
911016c	12.6	13.6	13.3	1.0	2.3	0.7	1.9	0.3	1.1
911019c	6.8	7.7	7.4	0.9	2.2	0.6	2.0	0.4	1.2
911025c	8.0	8.3	7.8	0.3	1.5	-0.2	1.0	0.5	1.2
911028c	8.8	8.3	7.4	-0.4	2.0	-1.4	1.1	0.9	1.3
911103c	13.0	15.1	13.9	2.1	2.5	0.9	2.1	1.2	1.3
911106c	10.0	12.5	12.0	2.5	3.6	2.0	3.8	0.4	1.1
911112c	9.5	10.1	9.3	0.5	2.1	-0.2	1.6	0.8	1.4
911115c	9.5	11.5	10.2	2.0	2.9	0.7	2.9	1.2	1.3
911121c	8.5	8.8	8.2	0.3	1.9	-0.3	1.7	0.6	1.1
911124c	10.4	11.2	10.0	0.8	2.8	-0.4	2.2	1.2	1.2
911130c	9.0	11.5	10.3	2.5	2.1	1.2	1.9	1.3	1.3
911203c	8.4	8.2	7.6	-0.2	2.2	-0.8	1.8	0.6	1.1
Statistics				0.8	2.3	0.3	2.0	0.5	1.0
neutral				0.1	2.4	0.3	2.0	-0.2	1.1
unstable									

Table 3: Comparison of VIERS and CMOD4 retrieved winds with analysed Meteo winds during CALVAL campaign.

4.2.2 *Qualitative analysis*

A qualitative analysis was performed on all data which were made available by ESA. This analysis led to a number of conclusions which were illustrated by four case studies in *Janssen et al* (1995). Here, we only discuss one case study, namely the detection and localisation of fronts, while also the main conclusions are summarised.

We study here briefly a case in which a large front is visible in the ERS-1 data. On the south western part of the front, the wind direction is south westerly, on the other side of the front the wind direction is north-easterly. Fig 14 shows the VIERS retrieved wind field on 6 November 1991 in large and the corresponding METEO and CMOD4 wind field in the subimages. When comparing the images a striking correspondence between on the one side the VIERS and CMOD4 result is seen while there is a clear discrepancy between the METEO winds and the ERS-1 derived winds. In the METEO wind field the front is not as pronounced as in the ERS-1 derived wind fields and the position is approximately 200 km north of the front observed by ERS-1.

This example illustrates the conclusion that the ERS-1 derived wind fields show more structure than the meteorological model fields. Furthermore, the difference between VIERS wind fields and CMOD4 wind fields is generally smaller than between ERS-1 derived winds and winds from the meteorological model. It should also be pointed out that the inversion method we employ is rather successful since the ERS-1 winds are quite different from the METEO winds which are used in the minimisation of the cost function D. An exception has to be made in case the METEO wind direction is orthogonal to the expected wind direction. In that event the inversion procedure is not always finding the right direction.

Additional observations we have inferred from studying the wind field maps are: 1) Because at small incidence angles the dependence on wind direction is weak the retrieved wind direction in cells with these small incidence angles is less reliable; fortunately, this only occurred in the cell with the smallest

incidence angle. 2) VIERS wind directions have a better internal consistency than CMOD4 directions, and 3) the VIERS model is capable of dealing with very low wind speeds.

Summarising, we conclude that the structure of the VIERS wind fields and CMOD4 wind fields is very similar indeed, while the difference between METEO and ERS-1 derived wind fields is bigger. This is probably related to the fact the METEO wind fields show much less structure than both the ones from VIERS and CMOD4. Once more, it may be concluded that the VIERS model is an acceptable algorithm to retrieve the wind vector from radar backscatter measurements.

5. CONCLUSION

We have developed a scatterometer algorithm based on the present understanding of the radar backscatter process and of the relevant processes governing the short wave spectrum. The final aim was to be able to obtain wind fields from the backscatter as observed by the scatterometer on board of satellites such as ERS-1.

Using observed wave spectra and observed backscatter in the laboratory it was readily realised that a simple two-scale model for the scattering process performed relatively well compared to other, more complicated models. In addition, it turned out that the short wave model was compatible with the wave measurements, in the sense that spectra sufficiently close to the measured ones could be generated by tuning parameters which were not fixed a priori. As a final result the two-scale model was combined with the wave model into the VIERS scatterometer algorithm. After a fine tuning exercise the algorithm evolved into the form described in this paper.

The present VIERS model has been shown to retrieve wind fields in a satisfactory manner; this followed both from the statistical comparison with ECMWF and CMOD4 wind fields and from the synoptic discussions. Furthermore, we have developed a method which enables us to retrieve in a cost-effective

way wind fields using a rather complicated and expensive algorithm such as VIERS is. In fact, it has been shown that in an operational environment retrieval of VIERS winds may be done as efficiently as with the present operational CMOD4 algorithm.

Although the retrieved winds from VIERS and CMOD4 are of comparable quality in a statistical sense, we found that compared to the ECMWF wind fields the CMOD4 winds are biased low in the high wind speed range. A similar conclusion follows from a comparison with buoy observations. The VIERS bias was much less in this range. It should be once more emphasized that a reliable retrieval of winds in the high wind speed range is important. A negative bias in the wind retrieval would result in a considerably less deep analysed depression since over the oceans the wind vector is related to a good approximation to the pressure gradient (geostrophic balance).

A weak point of the VIERS algorithm is the too simple directional distribution of the short waves. This is probably the major cause of the larger misfit in σ-space (when compared to CMOD4). The strong point of the VIERS algorithm, on the other hand, is that we have followed an approach based on physics. The framework of physical modelling as given by VIERS offers great potential for the future. Although CMOD4 at the moment shows a closer fit between modelled and observed backscatter, new insights into the directional distribution of the short waves will improve the performance of VIERS in this respect. Because of our framework this is a relatively easy step to take. In addition, in this way we were able to incorporate in a natural manner effects of sea state, slicks and atmospheric stability.

ACKNOWLEDGEMENT

Useful discussions with David Anderson, Tony Hollingsworth, Ad Stoffelen and Pete Woiceshyn are much appreciated. We thank J Onvlee for providing WAM model data during the CalVal campaign. This work was supported by the Dutch Remote Sensing Board (BCRS).

REFERENCES

Alpers, W and H Hühnerfuss, 1989: The damping of Ocean Waves by Surface Films: A New Look at an Old Problem. J Geophys Res, **94**, 6251-6265.

Anderson, D, A Hollingsworth, S Uppala and P Woiceshyn, 1987: A study on the feasibility of using sea and wind information from the ERS-1 satellite. ESA report part 1, ECMWF, Reading, 121 p.

Andersson, E, J Haseler, P Undén, P Courtier, G Kelly, D Vasiljevic, C Brankovic, C Cardinali, C Gaffard, A Hollingsworth, C Jakob, P Janssen, E Klinker, A Lanzinger, M Miller, F Rabier, A Simmons, B Strauss, J-N Thépaut and P Viterbo, 1996: The ECMWF implementation of three-dimensional variational assimilation (3D-Var). Part III: Experimental results.

Apel, J R, 1994: An improved model of the ocean surface wave vector spectrum and its effects on radar backscatter. J Geophys Res, **99**, 16269-16291.

Bahar, E, D E Barrick and M A Fitzwater, 1983: Computations of scattering cross sections for composite surfaces and the specification of the wave number where spectral splitting occurs. IEEE Trans Antennas and Propagation, **31** (5), 698-709.

Banner, M L, 1990: Equilibrium spectra of wind waves. J Phys Oceanogr, **20**, 966-984.

Barrick, D E and C T Swift, 1980: The seasat microwave instruments in historical perspective, IEEE J Oceanic Eng, OE-5(2), 74-79.

Brown, G S, 1978: Backscattering from a Gaussian distributed perfectly conducting rough surface. IEEE Trans Antennas and Propagation, **26** (3), 472-482.

Businger, J A, J C Wyngaard, I Izumi and E F Bradley, 1971: Flux-profile relationships in the atmospheric surface layer. J Atmosph Science, **28**, 181-189.

Calkoen, C J et al, 1990: Viers-1 progress report part 2. Technical Report BCRS 90-27, BCRS.

Davidson, R C, 1972: Methods in Nonlinear Plasma Theory, Academic.

Donelan, M A, J Hamilon and W H Hui, 1985: Directional spectra of wind-generated waves. Phil Trans R Soc Lond A315, 509-562.

Donelan, M A and W J Pierson, 1987: Radar scattering and equilibrium ranges in wind-generated waves with application to scatterometry. J Geophys Res, **92**, 4971-5029.

Dyer, A J and B B Hicks, 1970: Flux-gradient relationships in the constant flux layer. Q J Royal Meteorol Soc, **96**, 715-721.

Gaffard, C and H Roquet, 1995: Impact of the ERS-1 scatterometer wind data on the ECMWF 3D-Var assimilation system. ECMWF Technical Memorandum No. 217.

Guinard, N W, J T Ransone, Jr and J C Daley, 1971: Variation of the NCRS of the sea with increasing roughness. J Geophys Res, **76**, 1525-1538.

Günther, H, 1981: A parametric surface wave model and the statistics of the prediction parameters. PhD Thesis, University of Hamburg, 90 p.

Hasselmann, K, 1962: On the non-linear energy transfer in a gravity wave spectrum - Part 1. J Fluid Mech, **12**, 481-500.

Hasselmann, K, T P Barnett, E Bouws, H Carlson, D E Cartwright, K Enke, J A Ewing, H Gienapp, D E Hasselmann, P Kruseman, A Meerburg, P Müller, D J Olbers, K Richter, W Sell and H Walden, 1973: Measurements of wind-wave growh and swell decay during the Joint North Sea Wave Project (JONSWAP). Deutsch Hydrogr Z Suppl bf A8 (12), 95 p.

Jähne, B and K S Riemer, 1990: Two-dimensional wave number spectra of small-scale water surface waves. J Geophys Res Oceans, **95**, 11531-11546.

Janssen, P A E M, 1987: The initial evolution of gravity-capillary waves. J Fluid Mech, **184**, 581-597.

Janssen, P A E M, P Lionello and L Zambresky, 1989: On the interaction of wind and waves. Phyl Trans R Soc London, **A329**, 289-301.

Janssen, P A E M, C J Calkoen, D van Halsema, W A Oost, P Snoeij and H Wallbrink, 1995: VIERS-1 Final Report Phase 4.

Jones, W L, L C Schroeder and J L Mitchell, 1977: Aircraft measurements of the microwave scattering signature of the ocean, IEEE Trans Antennas and Propagation, AP-23, 52-61.

Jones, W L, F J Wentz and L C Schroeder, 1978: Algorithm for inferring wind stress from Seasat-A, AIAA J Spacecraft Rockets, **15**, 368-374.

Kitaigorodskii, S A, 1983: On the theory of the equilibrium range in the spectrum of wind-generated gravity waves. J Phys Oceanogr, **13**, 816-827.

Klinke, J and B Jähne, 1992: 2D wave number spectra of short wind waves - results from wind-wave facilities and extrapolation to the ocean. Proc of Conference on Optics of the Air-Sea interface, Theory and Measurements, L Estep ed, San Diego.

Komen, G J, K Hasselmann and S Hasselmann, 1984: On the existence of a fully developed wind-sea spectrum. J Phys Oceanogr, **14**, 1271-1285.

Komen, G J, L Cavaleri, M Donelan, K Hasselmann, S Hasselmann and P A E M Janssen, 1994: Dynamics and modelling of ocean waves, Cambridge University Press, Cambridge, 532 p.

Lamb, H, 1932: Hydrodynamics, 6th ed, Dover, New York, 738 p.

Lombardini, P P, 1986: Maximum of damping ratio in rippled water covered by monomolecular films. ONRL Report on the Role of Surfactant Films on the Interface Properties of the Sea Surface. F L Herr and J Williams, Eds, Office of Naval Research, London, Rep **C-11-86**, 157-173.

Moore, R J and A K Fung, 1979: Radar determination of winds at sea. Proc IEEE, **67**, 1504-1521.

Moore, R J and W J Pierson, 1967: Measuring sea state and estimating surface winds from a polar orbiting satellite, in Proceedings of the Symposium on Electromagnetic Sensing of the Earth from Satellites, edited by R Zirkland, pp R1-R28, Polytechnic Press, New York.

Phillips, O M, 1985: Spectral and statistical properties of the equilibrium range in wind-generated gravity waves. J Fluid Mech, **156**, 505-531.

Plant, W J, 1980: On the steady state energy balance of short gravity wave systems. J Phys Oceanogr, **10**, 1340-1352.

Plant, W J, 1990: In Surface Waves and Fluxes (Eds G L Geernaert and W L Plant). 2 Vols, Kluwer, Dordrecht.

Schroeder, L C, D M Boggs, G J Dome, I M Halberstam, W L Jones, W J Pierson and F J Wentz, 1982: The relationship between wind vector and normalised radar cross section used to derive Seasat-A satellite scatterometer winds. J Geophys Res, **87**, 3318-3336.

Stoffelen, A and D Anderson, 1996: Scatterometer data: Interpretation, estimation and validation of the transfer function CMOD4. To appear in J Geophys Res.

Smith, S D, R J Anderson, W A Oost, C Kraan, N Maat, J de Cosmo, K B Katsaros, K L Davidson, K Bumke, L Hasse and H H Chadwick, 1992: Sea surface wind stress and drag coefficients. The HEXOS results. Bound-Layer Meteor, **60**, 109-142.

Snoeij, P, E van Halsema, J Vogelzang, S Waas, S Zecchetto, H Janssen, W Oost, B Jähne, Ch Calkoen, 1993: VIERS-1 Final Report Phase 3. BCRS report 92-24.

Stewart, R H, 1985: Methods of satellite oceanography, University of California Press, 360 p.

Valenzuela, G R, M B Laing and J C Daley, 1971: Ocean spectra for the high-frequency waves as determined from airborne radar measurements, J Mar Res, **29**, 69-84.

Valenzuela, G R, 1978: Theories for the interaction of electromagnetic and oceanic waves - a review. Bound-Layer Meteor, **13**, 612-685.

Van Gastel, K, 1987: Nonlinear interactions of gravity-capillary waves: Lagrangian theory and effects on the spectrum. J Fluid Mech, **182**, 499-523.

Van Halsema, D et al, 1989: Progress report on the VIERS-1 project. Technical report BCRS 89-24, BCRS.

Wentz, F J, S Peteherych and L A Thomas, 1984: A model function for ocean radar cross sections at 14.6. GHZ J Geophys Res, **89**, 3689-3704.

Woiceshyn, P M, M G Wurtele, D H Boggs, L F McGoldrick and S Peteherych, 1986: The necessity for a new parametrization of an empirical model for wind/ocean scatterometry. J Geophys Res, **91**, 2273-2288.

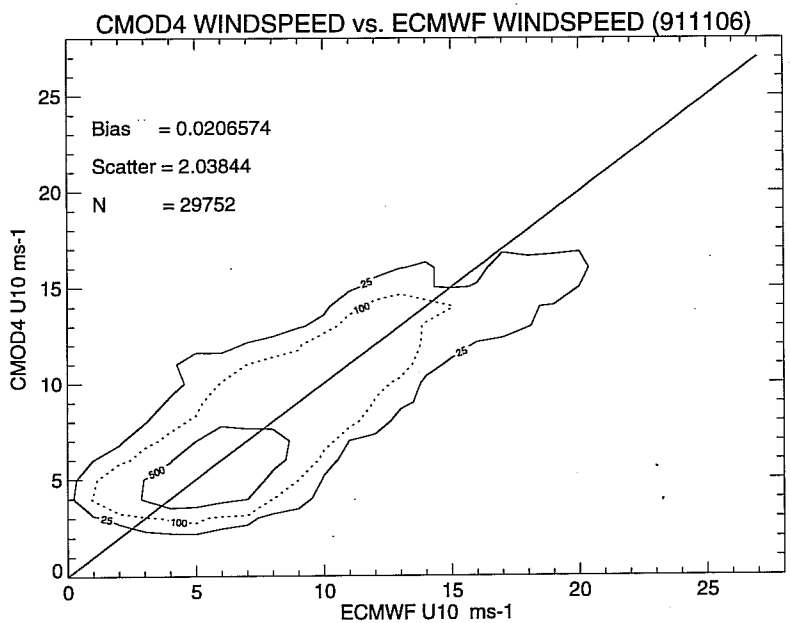

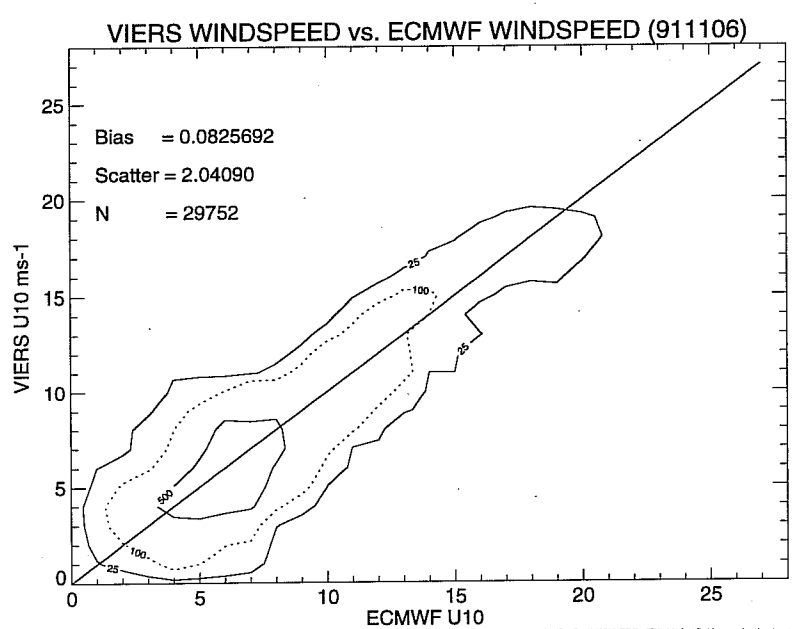

Fig.6 Retrieved wind speed using CMOD4 (top) and VIERS algorithme versus analysed ECMWF windspeed on 911106.

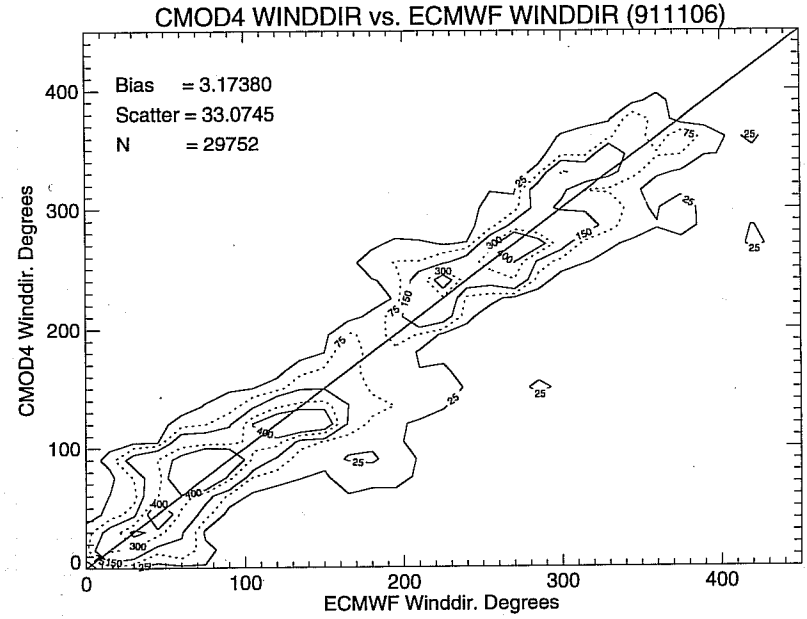

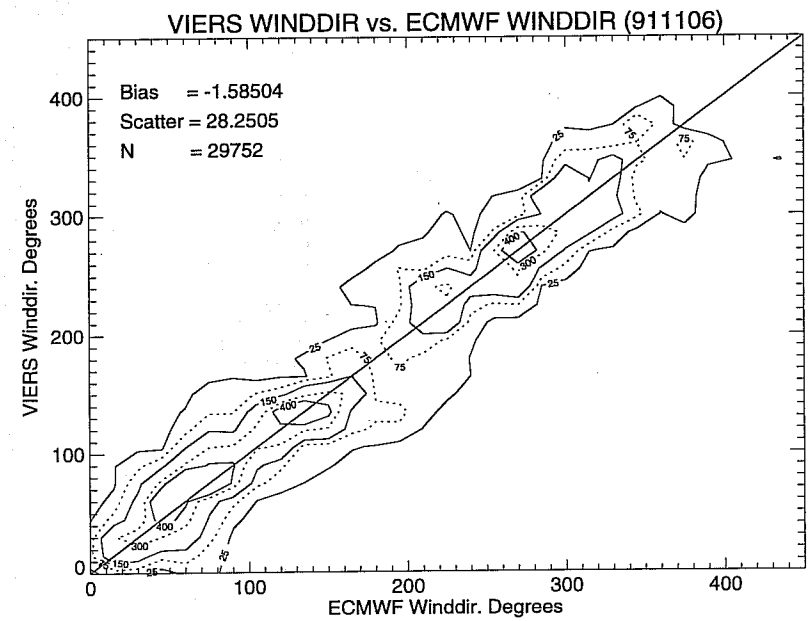

Fig.7 Same as Fig.6 but now for wind direction.

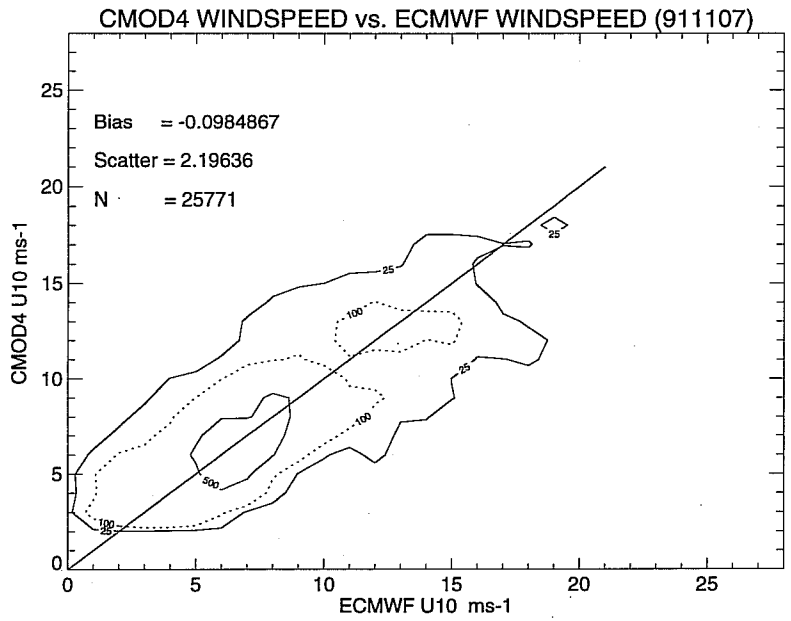

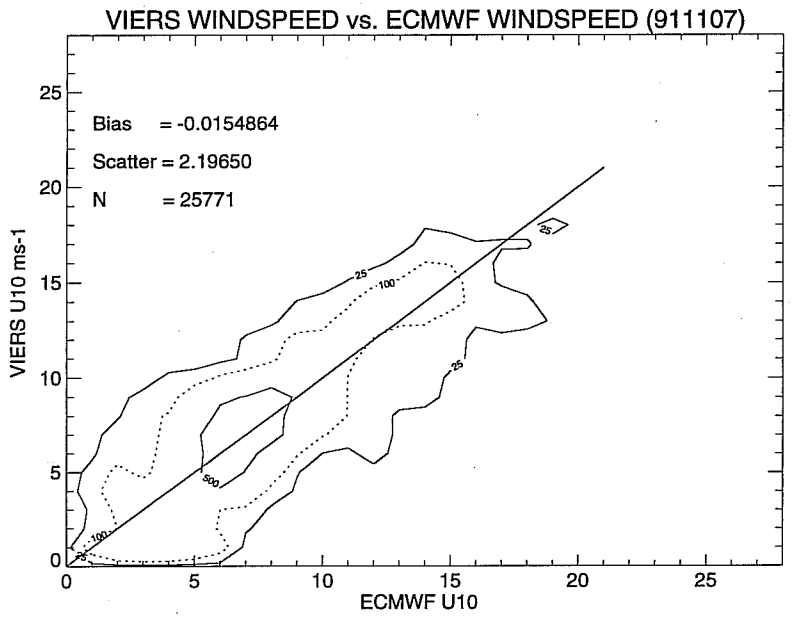

Fig.8 Same as Fig.6 but now for date 911107.

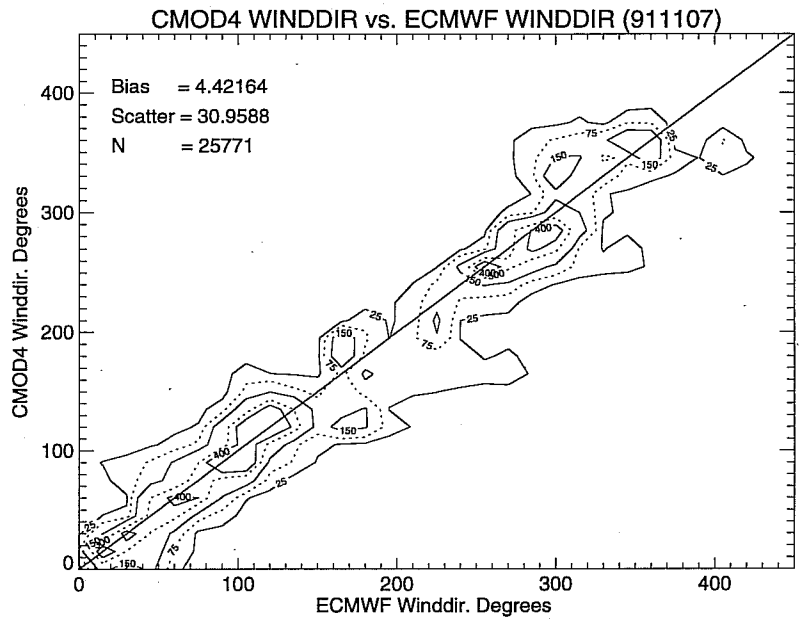

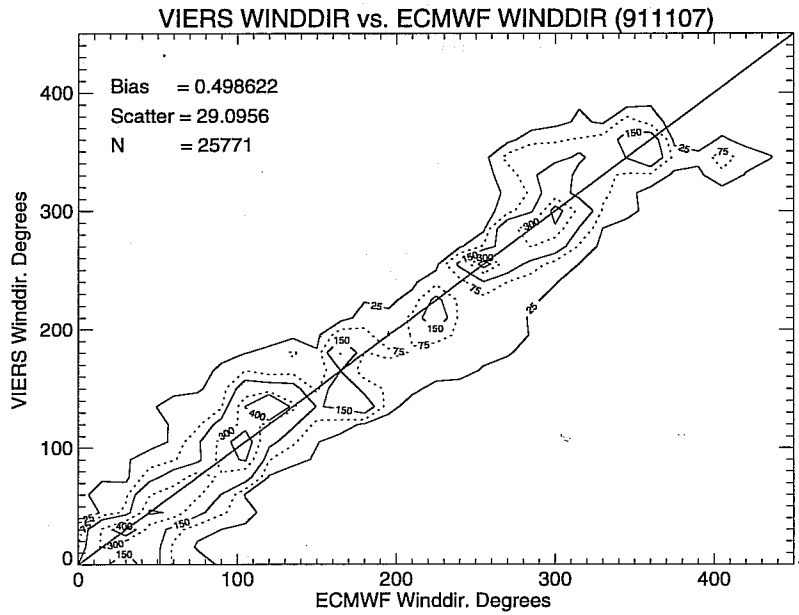

Fig.9 Same as Fig.7 but now for date 911107.

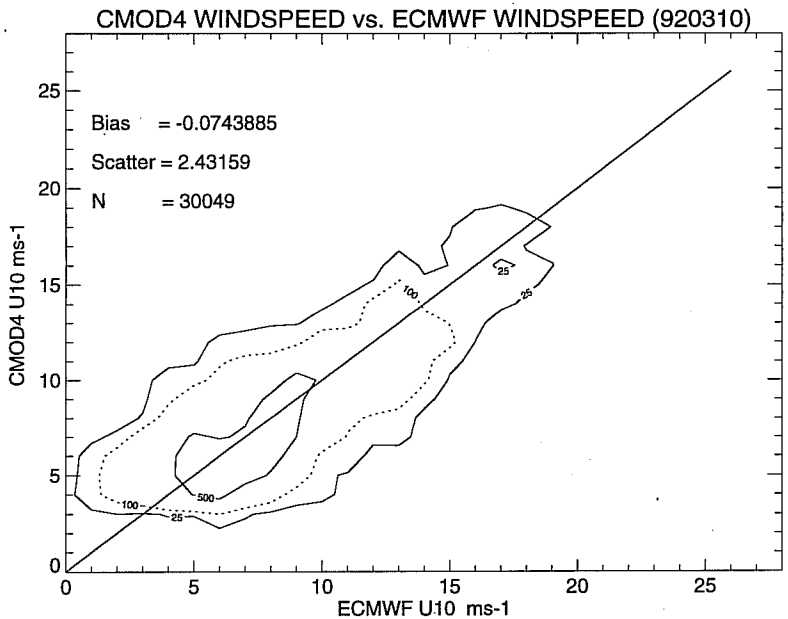

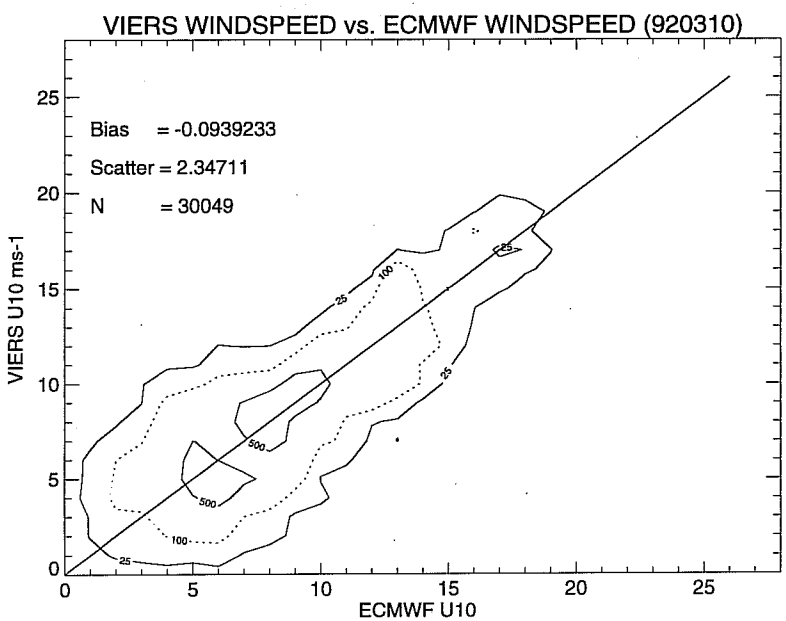

Fig.10 Same as Fig.6 but now for date 920310.

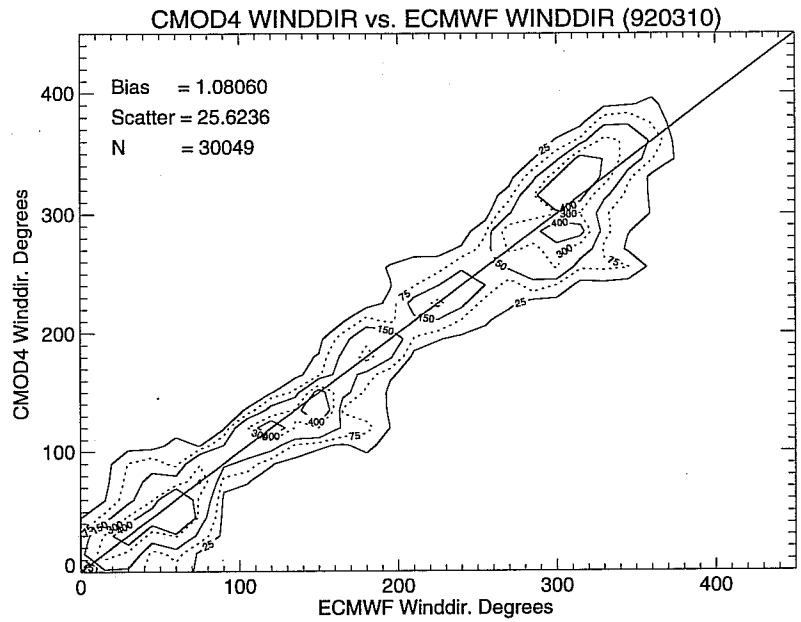

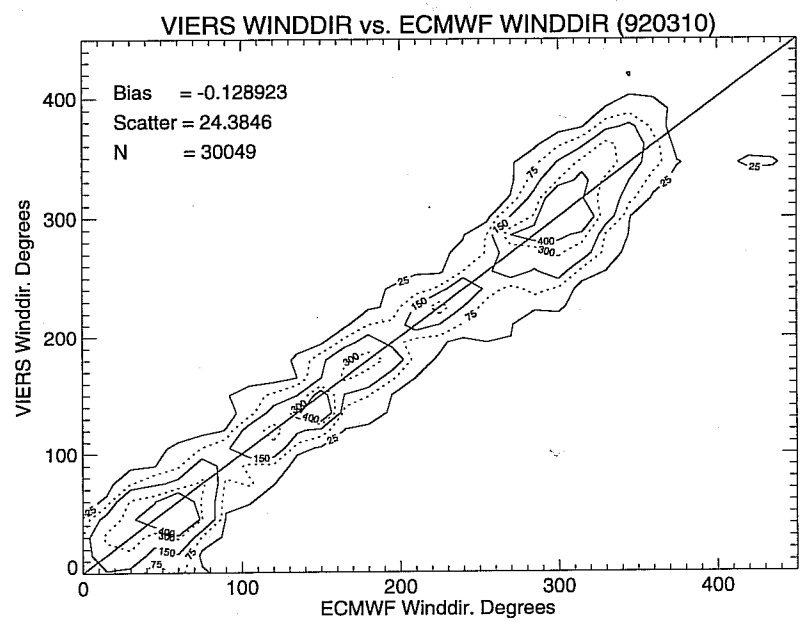

Fig.11 Same as Fig.7 but now for date 920310.

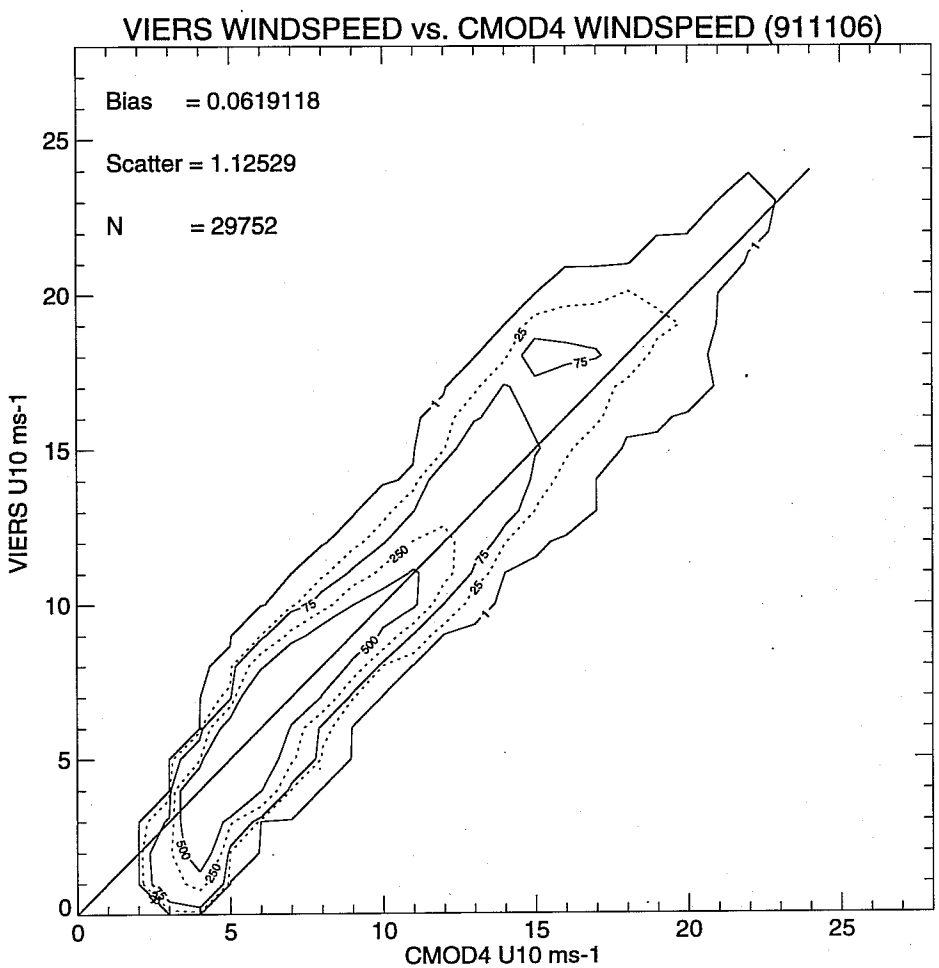

Fig.12 Comparison of VIERS and CMOD4 wind speed for 911106.

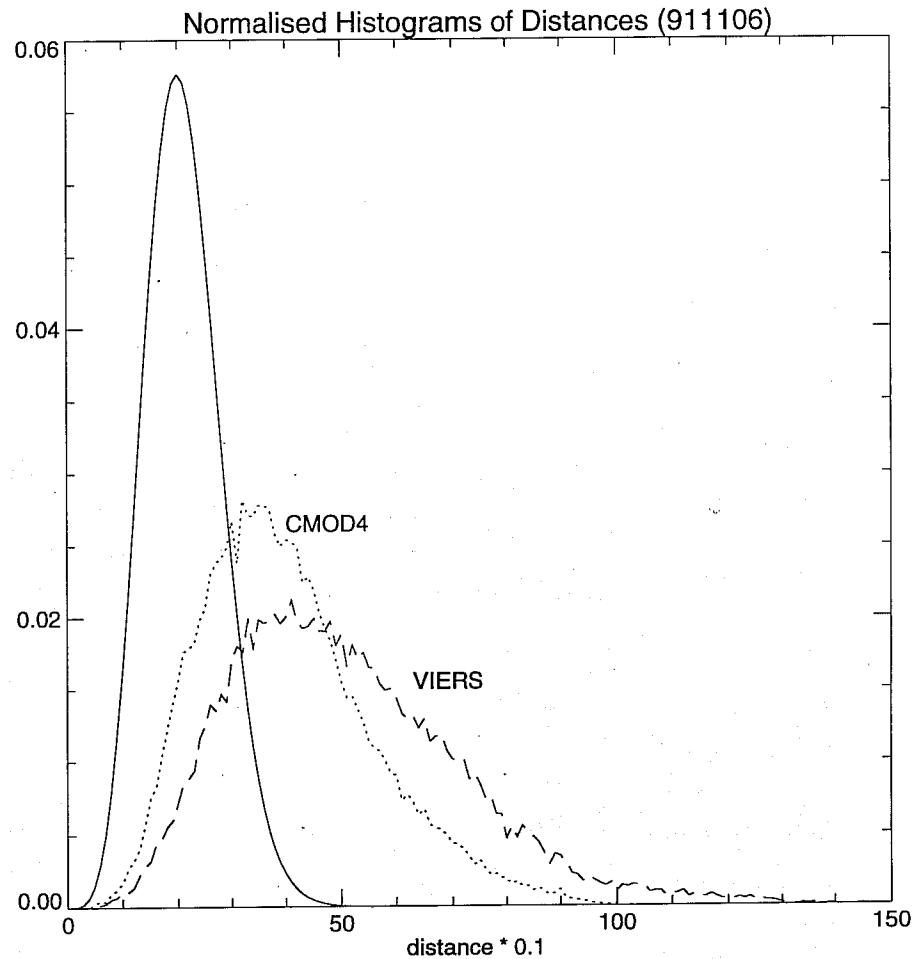

Fig.13 Normalised back scatter distance distribution for CMOD4 and VIERS. The distribution for a perfect model is shown as well.

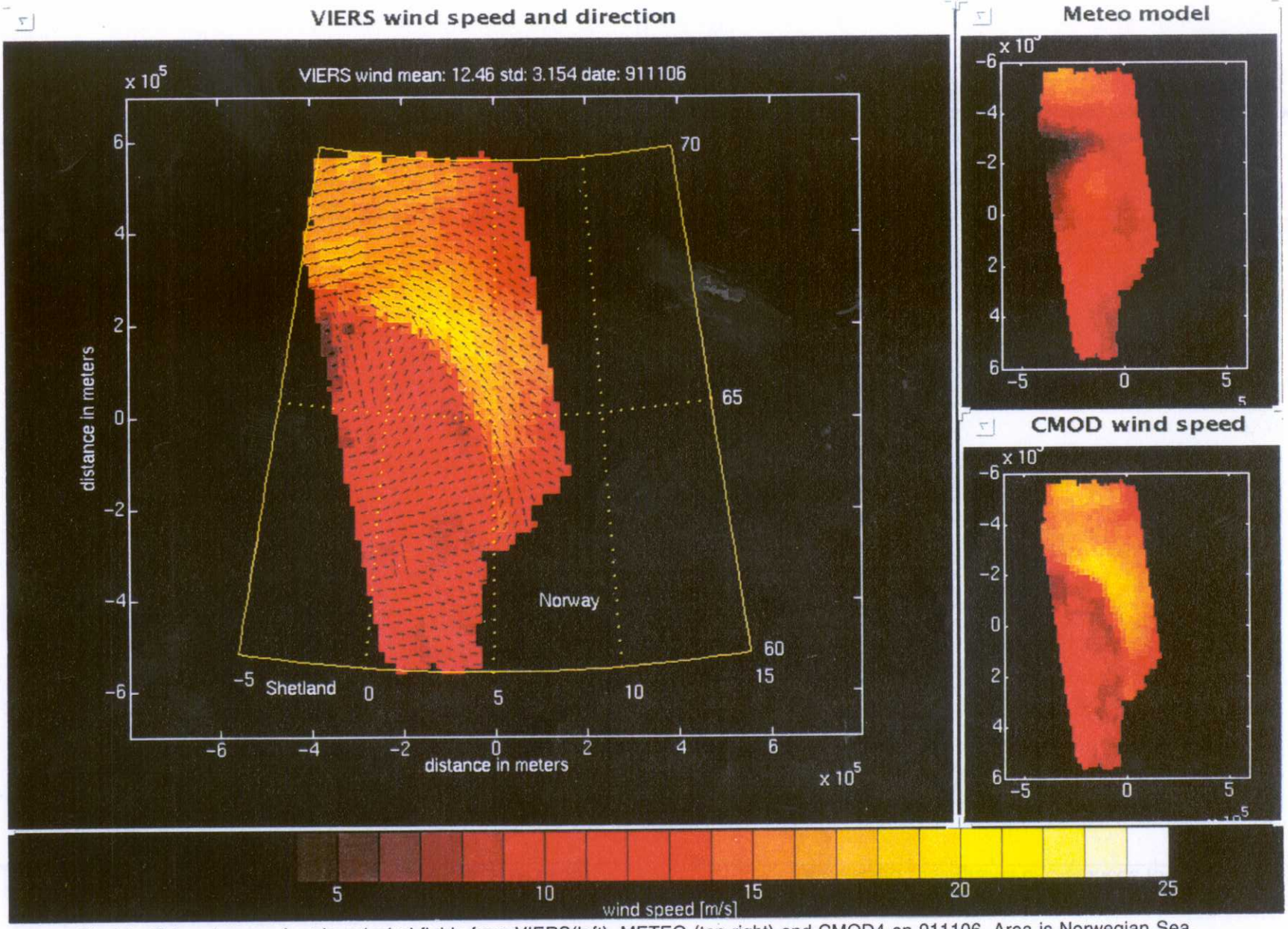

Fig.14 Colour image of retrieved wind fields from VIERS(left), METEO (top right) and CMOD4 on 911106. Area is Norwegian Sea.